arXiv:1701.06448v1 [math.NA] 20 Jan 2017

Variational integrators for anelastic and pseudo-incompressible flows

Werner Bauer[1,2] and François Gay-Balmaz[2]

Abstract

The anelastic and pseudo-incompressible equations are two well-known soundproof approximations of compressible flows useful for both theoretical and numerical analysis in meteorology, atmospheric science, and ocean studies. In this paper, we derive and test structure-preserving numerical schemes for these two systems. The derivations are based on a discrete version of the Euler-Poincaré variational method. This approach relies on a finite dimensional approximation of the (Lie) group of diffeomorphisms that preserve *weighted*-volume forms. These weights describe the background stratification of the fluid and correspond to the weighed velocity fields for anelasic and pseudo-incompressible approximations. In particular, we identify to these discrete Lie group configurations the associated Lie algebras such that elements of the latter correspond to weighted velocity fields that satisfy the divergence-free conditions for both systems. Defining discrete Lagrangians in terms of these Lie algebras, the discrete equations follow by means of variational principles. We verify the structure-preserving nature of the resulting variational integrators applying two test cases. The spectra of internal gravity waves, emitted by a hydrostatic adjustment process, perfectly reflects the models' dispersion relations. And, shape and advection speed of a rising and a falling bubble match very well reference results in literature. Descending from variational principles, the schemes exhibit further a discrete version of Kelvin circulation theorem, are applicable to irregular meshes, and show excellent long term energy behavior.

1 Introduction

Numerical simulations of atmosphere and ocean on the global scale are of high importance in the field of Geophysical Fluid Dynamics (GFD). The dynamics of these systems are frequently modeled by the full Euler equations using explicit time integration schemes (see, e.g., [6]). These simulations are however computationally very expensive. Besides highly resolved meshes to capture important small scale features, the fast traveling sound waves have to be resolved too, by very small time step sizes, in order to guarantee stable simulations [6]. As these sound wave are assumed to be negligible in atmospheric flows, soundproof models, in which these fast waves are filtered out, are a viable option that permits to increase the time step sizes and hence to speed up calculations significantly.

[1]Imperial College London, Department of Mathematics, 180 Queen's Gate, London SW7 2AZ, United Kingdom. w.bauer@imperial.ac.uk

[2]École Normale Supérieure/CNRS, Laboratoire de Météorologie Dynamique, Paris, France. gaybalma@lmd.ens.fr

Frequently applied soundproof models are the Boussinesq, anelastic, pseudo-incompressible approximations of the Euler equations [5, 11, 13]. There exist elaborated discretizations of these equations in literature. However, these discretizations often do not take into account the underlying geometrical structure of the equations. This may result in a lack of conserving mass, momentum, energy, or to the fact that the Helmholtz decomposition of vector fields or the Kelvin-Noether circulation theorem are not satisfied. Structure-preserving schemes descending from Euler-Poincaré variational methods [14], [7], [4] conserve these quantities, as they arise from a Lagrangian formulation, in which these conserved quantities are given by invariants of the Lagrangian under symmetries, [8].

With this paper, we contribute to develop variational integrators in the area of GFD by including the anelastic and pseudo-incompressible schemes into the variational discretization framework developed by [14]. To use this framework, we first have to describe the approximation of the Euler equations for a perfect fluid in terms of the Euler-Poincaré variational method [8]. The central idea is to use volume forms that are weighted by the corresponding background stratifications such that they match the divergence-free conditions of the correspondingly weighed velocity fields associated to either the anelastic or the pseudo-incompressible approximations. This will allow us to identify for these approximations the appropriate Lie group configuration with corresponding Lie algebras. Using the latter to define appropriate Lagrangian, the equations of motion follow by Hamilton's variational principle of stationary action.

The definition of appropriate discrete diffeomorphism groups will be based on the idea to use weighted meshes that provide discrete counterparts of the weighted volume forms. The corresponding discrete Lie algebras will incorporate the required divergence-free conditions on the weighed velocity fields. Defining appropriate weighted pairings required to derive the functional derivatives of the discrete Lagrangians, the flat operator introduced in [14] is directly applicable and we can thus avoid to discuss this otherwise delicate issue. Mimicking the continuous theory, the discretizations of anelastic and pseudo-incompressible equations follow by variations of appropriate discrete Lagrangians.

We structure the paper as follows. In Section 2 we recall the standard formulations of Boussinesq, anelastic, and pseudo-incompressible approximations of the Euler equations for perfect fluids. In Section 3 we show that these formulations follow for appropriate Langrangians from the Euler-Poincaré variational principle. In Section 4 we recall the variational discretization framework introduced by [14] and extend it to suit anelastic and pseudo-incompressible equations. In Section 5 we derive corresponding discretizations on 2D simplicial meshes and provide explicit formulations in terms of velocity and buoyancy or potential temperature fields. In Section 6 we perform numerical tests to demonstrate the structure-preserving properties of the variational integrators. In Section 7 we draw conclusions and provide an outlook.

2 Anelastic and pseudo-incompressible systems

In this section we review the three approximations of the Euler equations of a perfect gas that will be the subject of this paper, namely, the Boussinesq, the anelastic, and the pseudo-incompressible approximations (see, e.g., [6] for more details).

The Euler equations for the inviscid isentropic motion of a perfect gas can be expressed in

the form

$$\partial_t \mathbf{u} + \mathbf{u}\cdot\nabla\mathbf{u} + \frac{1}{\rho}\nabla p = -g\mathbf{z}, \quad \partial_t \rho + \operatorname{div}(\rho\mathbf{u}) = 0, \quad \partial_t \theta + \mathbf{u}\cdot\nabla\theta = 0, \tag{2.1}$$

where $\mathbf{u}$ is the three-dimensional velocity vector, ρ is the mass density, p is the pressure, g is the gravitational acceleration, $\mathbf{z}$ is the unit vector directed opposite to the gravitational force. The variable θ is the potential temperature, defined by $\theta = T/\pi$, in which T is the temperature and π is the Exner pressure

$$\pi = (p/p_0)^{R/c_p},$$

with R is the gas constant for dry air, c_p is the specific heat at constant pressure, and p_0 is a constant reference pressure. Using the equation of state for a perfect gas, $p = \rho RT$, we have the relation

$$\frac{1}{\rho}\nabla p = c_p \theta \nabla \pi.$$

The equations (2.1) correspond to conservation of momentum, mass, and entropy, respectively.

Let us write

$$\theta(x,y,z,t) = \bar{\theta}(z) + \theta'(x,y,z,t), \quad \pi(x,y,z,t) = \bar{\pi}(z) + \pi'(x,y,z,t),$$

in which $\bar{\theta}(z)$ and $\bar{\pi}(z)$ characterize a vertically varying reference state in hydrostatic balance, that is,

$$c_p \bar{\theta} \frac{d\bar{\pi}}{dz} = -g. \tag{2.2}$$

In terms of the perturbations θ' and π', the equations (2.1) can be equivalently written as

$$\partial_t \mathbf{u} + \mathbf{u}\cdot\nabla\mathbf{u} + c_p\theta\nabla\pi' = g\frac{\theta'}{\bar{\theta}}\mathbf{z}, \quad \partial_t \rho + \operatorname{div}(\rho\mathbf{u}) = 0, \quad \partial_t \theta + \mathbf{u}\cdot\nabla\theta = 0. \tag{2.3}$$

We introduce now three frequently applied approximations to these equations.

Boussinesq approximation. This approximation is obtained by assuming a nondivergent flow and by neglecting the variations in potential temperature except in the leading-order contribution to the buoyancy. We thus get, from (2.3), the system

$$\partial_t \mathbf{u} + \mathbf{u}\cdot\nabla\mathbf{u} + c_p\theta_0\nabla\pi' = g\frac{\theta'}{\theta_0}\mathbf{z}, \quad \operatorname{div}\mathbf{u} = 0, \quad \partial_t\theta + \mathbf{u}\cdot\nabla\theta = 0,$$

in which θ_0 is a constant reference potential temperature. These equations can equivalently be written as

$$\partial_t \mathbf{u} + \mathbf{u}\cdot\nabla\mathbf{u} + \nabla P_{\mathrm{b}}' = b'\mathbf{z}, \quad \operatorname{div}\mathbf{u} = 0, \quad \partial_t b' + \mathbf{u}\cdot\nabla b' + N^2 w = 0,$$

where $P_{\mathrm{b}}' = c_p\theta_0\pi'$, $N^2 = \frac{g}{\theta_0}\partial_z\bar{\theta}$ is the Brunt-Väisälä frequency, and $b' = g\frac{\theta'}{\theta_0}$ is the buoyancy. Making use of the full buoyancy $b = g\frac{\theta}{\theta_0} = g\frac{\bar{\theta}+\theta'}{\theta_0}$, we can write the system as

$$\partial_t \mathbf{u} + \mathbf{u}\cdot\nabla\mathbf{u} + \nabla P_{\mathrm{b}} = b\mathbf{z}, \quad \operatorname{div}\mathbf{u} = 0, \quad \partial_t b + \mathbf{u}\cdot\nabla b = 0, \tag{2.4}$$

where $P_{\mathrm{b}} := P_{\mathrm{b}}' + \frac{g}{\theta_0}\int_0^z \bar{\theta}(z)dz$.

The total energy is conserved since the energy density $E = \frac{1}{2}|\mathbf{u}|^2 - bz = \frac{1}{2}|\mathbf{u}|^2 - g\frac{\theta}{\theta_0}z$ verifies the continuity equation

$$\partial_t E + \operatorname{div}((E + P_{\mathrm{b}})\mathbf{u}) = 0. \tag{2.5}$$

The requirement for nondivergent flow is easily justified only for liquids, and the errors incurred approximating the true mass conservation relation by $\operatorname{div}\mathbf{u} = 0$ can be quite large in stratified compressible flows. In this case, the anelastic and pseudo-incompressible models have to be considered, which better approximate the true mass continuity equation.

Anelastic approximation. The anelastic system approximates the continuity equation as

$$\operatorname{div}(\bar{\rho}\mathbf{u}) = 0,$$

where $\bar{\rho}(z)$ is the vertically varying density of the reference state.

In the original anelastic system presented by [13], the reference state is isentropic so that $\bar{\theta}(z) = \theta_0$ is constant, which results in the approximation

$$\partial_t \mathbf{u} + \mathbf{u}\cdot\nabla\mathbf{u} + c_p\theta_0\nabla\pi' = g\frac{\theta'}{\theta_0}\mathbf{z}, \quad \operatorname{div}(\bar{\rho}\mathbf{u}) = 0, \quad \partial_t\theta + \mathbf{u}\cdot\nabla\theta = 0. \tag{2.6}$$

The energy density can be written as $E = \bar{\rho}\left(\frac{1}{2}|\mathbf{u}|^2 - g\frac{\theta}{\theta_0}z\right) = \bar{\rho}\left(\frac{1}{2}|\mathbf{u}|^2 + c_p\bar{\pi}\theta\right)$, where $\bar{\pi}(z) = -\frac{g}{c_p\theta_0}z$ verifies the hydrostatic balance (2.2) for $\bar{\theta}(z) = \theta_0$. The total energy is conserved since E verifies the continuity equation

$$\partial_t E + \operatorname{div}((E + P_{\mathrm{a}_0})\mathbf{u}) = 0$$

with $P_{\mathrm{a}_0} := \bar{\rho}(c_p\theta_0\pi' + gz)$

In the subsequent work [15], the reference potential temperature $\bar{\theta}$ was allowed to vary in the vertical, leading to the momentum equation

$$\partial_t \mathbf{u} + \mathbf{u}\cdot\nabla\mathbf{u} + c_p\bar{\theta}\nabla\pi' = g\frac{\theta'}{\bar{\theta}}\mathbf{z}.$$

The resulting system is however not energy conservative. In order to restore energy conservation, [11] considered the approximate momentum equation

$$\partial_t \mathbf{u} + \mathbf{u}\cdot\nabla\mathbf{u} + \nabla(c_p\bar{\theta}\pi') = g\frac{\theta'}{\bar{\theta}}\mathbf{z}, \quad \operatorname{div}(\bar{\rho}\mathbf{u}) = 0, \quad \partial_t\theta + \mathbf{u}\cdot\nabla\theta = 0. \tag{2.7}$$

In this case, the energy density $E = \bar{\rho}\left(\frac{1}{2}|\mathbf{u}|^2 + c_p\bar{\pi}\theta\right)$, where $\bar{\pi}(z)$ is such that $c_p\frac{\partial\bar{\pi}}{\partial z} = -\frac{g}{\bar{\theta}}$, satisfies the continuity equation

$$\partial_t E + \operatorname{div}((E + P_{\mathrm{a}})\mathbf{u}) = 0,$$

with $P_{\mathrm{a}} := \bar{\rho}(c_p\bar{\theta}\pi' + gz)$.

Pseudo-incompressible approximation. To obtain this approximation developed in [5], one defines the pseudo-density $\rho^* = \bar{\rho}\bar{\theta}/\theta$ and enforces mass conservation with respect to ρ^* as $\partial_t \rho^* + \mathrm{div}(\rho^* \mathbf{u}) = 0$. When combined with $\partial_t \theta + \mathbf{u} \cdot \nabla \theta = 0$, it yields $\mathrm{div}(\bar{\rho}\bar{\theta}\mathbf{u}) = 0$. These last two equations can be used with the momentum equation in (2.3) to yield the energy conservative system

$$\partial_t \mathbf{u} + \mathbf{u} \cdot \nabla \mathbf{u} + c_p \theta \nabla \pi' = g \frac{\theta'}{\bar{\theta}} \mathbf{z}, \quad \mathrm{div}(\bar{\rho}\bar{\theta}\mathbf{u}) = 0, \quad \partial_t \theta + \mathbf{u} \cdot \nabla \theta = 0. \tag{2.8}$$

We note that the balance of momentum is equivalently written as $\partial_t \mathbf{u} + \mathbf{u} \cdot \nabla \mathbf{u} + c_p \theta \nabla \pi = -g\mathbf{z}$, where $\pi = \bar{\pi} + \pi'$, with $c_p \frac{\partial \bar{\pi}}{\partial z} = -\frac{g}{\bar{\theta}}$. The energy density $E = \rho^* \left(\frac{1}{2}|\mathbf{u}|^2 + gz \right)$ verifies the continuity equation

$$\partial_t E + \mathrm{div}((E + P_{\mathrm{pi}})\mathbf{u}) = 0$$

for $P_{\mathrm{pi}} := c_p \rho^* \theta \pi$.

3 Variational formulation

We shall now formulate the anelastic and pseudo-incompressible equations in Euler-Poincaré variational form. Euler-Poincaré variational principles are Eulerian versions of the classical Hamilton principle of critical action. We refer to [8] for the general Euler-Poincaré theory based on Lagrangian reduction and for several applications in fluid dynamics. An Euler-Poincaré formulation for anelastic systems was given in [3]. We shall develop below a slightly different Euler-Poincaré approach, well-suited for the variational discretization, by putting the emphasis on the underlying Lie group of diffeomorphisms associated to these systems.

As we have recalled above, the anelastic and pseudo-incompressible equations are based on a constraint of the following type on the fluid velocity $\mathbf{u}(t, \mathbf{x})$:

$$\mathrm{div}(\bar{\sigma}\mathbf{u}) = 0,$$

for a given strictly positive function $\bar{\sigma}(\mathbf{x}) > 0$ on the fluid domain $\mathcal{D}$.

We assume that the fluid domain $\mathcal{D}$ is a compact, connected, orientable manifold with smooth boundary $\partial\mathcal{D}$. In our examples, $\mathcal{D}$ is a 2D domain in the vertical plane $\mathbb{R}^2 \ni \mathbf{x} = (x, z)$ or a 3D domain in $\mathbb{R}^3 \ni \mathbf{x} = (x, y, z)$.

We fix a volume form μ on $\mathcal{D}$, i.e., an n-form, $n = \dim \mathcal{D}$, with $\mu(\mathbf{x}) \neq 0$, for all $\mathbf{x} \in \mathcal{D}$. If $\mathcal{D}$ is a domain in $\mathbb{R}^3 \ni (x, y, z)$, one can take $\mu = dx \wedge dy \wedge dz$ to be the standard volume of $\mathbb{R}^3$ restricted to $\mathcal{D}$. We shall denote by $\mathrm{div}_\mu(\mathbf{u})$ the divergence of $\mathbf{u}$ with respect to the volume form μ. Recall that the divergence is the function $\mathrm{div}_\mu(\mathbf{u})$ defined by the equality

$$\pounds_{\mathbf{u}} \mu = \mathrm{div}_\mu(\mathbf{u}) \mu,$$

in which $\pounds_{\mathbf{u}}$ denotes the Lie derivative with respect to the vector field $\mathbf{u}$, see, e.g., [1]. When μ is the standard volume, one evidently recovers the usual divergence operator div on vector fields.

Diffeomorphism groups. Let us denote by $\mathrm{Diff}_\mu(\mathcal{D})$ the group of all smooth diffeomorphisms $\varphi : \mathcal{D} \to \mathcal{D}$ that preserve the volume form μ, i.e., $\varphi^* \mu = \mu$. The group structure on $\mathrm{Diff}_\mu(\mathcal{D})$ is given by the composition of diffeomorphisms. The group $\mathrm{Diff}_\mu(\mathcal{D})$ can be endowed with the structure of a Fréchet Lie group, although in this paper we shall only use the Lie group

structure at a formal level. The Lie algebra of the group $\mathrm{Diff}_\mu(\mathcal{D})$ is given by the space $\mathfrak{X}_\mu(\mathcal{D})$ of all divergence free (relative to μ) vector fields on $\mathcal{D}$, parallel to the boundary $\partial\mathcal{D}$:

$$\mathfrak{X}_\mu(\mathcal{D}) = \{\mathbf{u} \in \mathfrak{X}(\mathcal{D}) \mid \mathrm{div}_\mu(\mathbf{u}) = 0, \quad \mathbf{u} \parallel \partial\mathcal{D}\}.$$

Given the strictly positive function $\bar{\sigma} > 0$ on $\mathcal{D}$, we consider the new volume form $\bar{\sigma}\mu$ with associated diffeomorphism group and Lie algebra denoted $\mathrm{Diff}_{\bar{\sigma}\mu}(\mathcal{D})$ and $\mathfrak{X}_{\bar{\sigma}\mu}(\mathcal{D}) = \{\mathbf{u} \in \mathfrak{X}(\mathcal{D}) \mid \mathrm{div}_{\bar{\sigma}\mu}(\mathbf{u}) = 0, \quad \mathbf{u} \parallel \partial\mathcal{D}\}$, respectively. In the next Lemma, we rewrite the condition $\mathrm{div}_{\bar{\sigma}\mu}(\mathbf{u}) = 0$ by using exclusively the divergence operator div_μ associated to the initial volume form μ.

Lemma 3.1 *Let $\mathcal{D}$ be a manifold endowed with a volume form μ and let $\bar{\sigma} > 0$ be a strictly positive smooth function on $\mathcal{D}$. Then we have*

$$\mathrm{div}_\mu(\bar{\sigma}\mathbf{u}) = \bar{\sigma}\,\mathrm{div}_{\bar{\sigma}\mu}(\mathbf{u}).$$

Proof. We will use the following properties of the Lie derivative $\pounds_{\mathbf{u}}$, the exterior differential $\mathbf{d}$, and the inner product $\mathbf{i}_{\mathbf{u}}$ on differential forms (see, e.g., [1]): for a k-form α, an n-form β, and a vector field $\mathbf{u}$, we have

$$\begin{aligned}
&\pounds_{\mathbf{u}}\alpha = \mathbf{d}\left(\mathbf{i}_{\mathbf{u}}\alpha\right) + \mathbf{i}_{\mathbf{u}}\mathbf{d}\alpha, \quad \mathbf{d}(\alpha \wedge \beta) = \mathbf{d}\alpha \wedge \beta + (-1)^k \alpha \wedge \mathbf{d}\beta,\\
&\mathbf{i}_{\mathbf{u}}(\alpha \wedge \beta) = \mathbf{i}_{\mathbf{u}}\alpha \wedge \beta + (-1)^k \alpha \wedge \mathbf{i}_{\mathbf{u}}\beta.
\end{aligned}$$

On the one hand, we have

$$\begin{aligned}
\mathrm{div}_\mu(\bar{\sigma}\mathbf{u})\mu = \pounds_{\bar{\sigma}\mathbf{u}}\mu = \mathbf{d}\left(\mathbf{i}_{\bar{\sigma}\mathbf{u}}\mu\right) = \mathbf{d}\left(\bar{\sigma}\mathbf{i}_{\mathbf{u}}\mu\right) = \mathbf{d}\bar{\sigma} \wedge \mathbf{i}_{\mathbf{u}}\mu + \bar{\sigma}\mathbf{d}\left(\mathbf{i}_{\mathbf{u}}\mu\right)\\
= \left(\mathbf{i}_{\mathbf{u}}\mathbf{d}\bar{\sigma}\right)\mu - \mathbf{i}_{\mathbf{u}}\left(\mathbf{d}\bar{\sigma} \wedge \mu\right) + \bar{\sigma}\,\mathrm{div}_\mu\,\mathbf{u} = \left(\mathbf{d}\bar{\sigma} \cdot \mathbf{u}\right)\mu + \bar{\sigma}\,\mathrm{div}_\mu\,\mathbf{u}.
\end{aligned}$$

On the other hand, we have

$$\bar{\sigma}\,\mathrm{div}_{\bar{\sigma}\mu}(\mathbf{u})\mu = \pounds_{\mathbf{u}}(\bar{\sigma}\mu) = \left(\mathbf{d}\bar{\sigma} \cdot \mathbf{u}\right)\mu + \bar{\sigma}\pounds_{\mathbf{u}}\mu = \left(\mathbf{d}\bar{\sigma} \cdot \mathbf{u}\right)\mu + \bar{\sigma}\,\mathrm{div}_\mu(\mathbf{u}).$$

This proves the result. ■

From this Lemma, we deduce that the appropriate Lie groups associated to the anelastic and pseudo-incompressible systems are given by

$$G = \mathrm{Diff}_{\bar{\rho}\mu}(\mathcal{D}) \quad \text{and} \quad G = \mathrm{Diff}_{\bar{\rho}\bar{\theta}\mu}(\mathcal{D}),$$

respectively. Indeed, from the preceding Lemma, it follows that the Lie algebras of these groups can be written as

$$\begin{aligned}
\mathfrak{X}_{\bar{\rho}\mu}(\mathcal{D}) &= \{\mathbf{u} \in \mathfrak{X}(\mathcal{D}) \mid \mathrm{div}_\mu(\bar{\rho}\mathbf{u}) = 0, \quad \mathbf{u} \parallel \partial\mathcal{D}\} \text{ and}\\
\mathfrak{X}_{\bar{\rho}\bar{\theta}\mu}(\mathcal{D}) &= \{\mathbf{u} \in \mathfrak{X}(\mathcal{D}) \mid \mathrm{div}_\mu(\bar{\rho}\bar{\theta}\mathbf{u}) = 0, \quad \mathbf{u} \parallel \partial\mathcal{D}\},
\end{aligned}$$

respectively. They correspond to the anelastic and pseudo-incompressible constraints on the fluid velocity. We will continue to uses the subscript $\bar{\sigma}\mu$ when referring to both Lie groups and both Lie algebras.

Euler-Poincaré variational principles. The diffeomorphism group $\mathrm{Diff}_{\bar\sigma\mu}(\mathcal{D})$ plays the role of the configuration manifold for these fluid models. The motion of the fluid is completely characterized by a time dependent curve $\varphi(t,_) \in \mathrm{Diff}_{\bar\sigma\mu}(\mathcal{D})$: a particle located at a point $X \in \mathcal{D}$ at time $t = 0$ travels to $\mathbf{x} = \varphi(t, X) \in \mathcal{D}$ at time t. Exactly as in classical mechanics, the Lagrangian of the system is defined on the tangent bundle $T\,\mathrm{Diff}_{\bar\sigma\mu}(\mathcal{D})$ of the configuration manifold. We shall denote it by $L_{\Theta_0} : T\,\mathrm{Diff}_{\bar\sigma\mu}(\mathcal{D}) \to \mathbb{R}$. The index Θ_0 indicates that this Lagrangian parametrically depends on the potential temperature $\Theta_0(X)$ that is expressed here in the Lagrangian description.

The equations of motion in the Lagrangian description follow from the Hamilton principle

$$\delta \int_0^T L_{\Theta_0}(\varphi, \dot\varphi)dt = 0, \tag{3.1}$$

over a time interval $[0, T]$, for variations $\delta\varphi$ with $\delta\varphi(0) = \delta\varphi(T) = 0$.

In the Eulerian description, the variables are the Eulerian velocity $\mathbf{u}(t, \mathbf{x})$ and the potential temperature $\theta(t, \mathbf{x})$. They are related to $\varphi(t, X)$ and $\Theta_0(X)$ as

$$\mathbf{u}(t, \varphi(t, X)) = \dot\varphi(t, X) \quad \text{and} \quad \theta(t, \varphi(t, X)) = \Theta_0(X). \tag{3.2}$$

We assume that the Lagrangian L_{Θ_0} can be rewritten exclusively in terms of these two Eulerian variables, and we denote it by $\ell(\mathbf{u}, \theta)$. This assumption means that L_{Θ_0} is right-invariant with respect to the action of the subgroup

$$\mathrm{Diff}_{\bar\sigma\mu}(\mathcal{D})_{\Theta_0} = \{\varphi \in \mathrm{Diff}_{\bar\sigma\mu}(\mathcal{D}) \mid \Theta_0(\varphi(X)) = \Theta_0(X),\ \forall\, X \in \mathcal{D}\}$$

of all diffeomorphisms that keep Θ_0 invariant.

By rewriting the Hamilton principle (3.1) in terms of the Eulerian variables $\mathbf{u}$ and θ, we get the Euler-Poincaré variational principle

$$\delta \int_0^T \ell(\mathbf{u}, \theta)dt = 0, \quad \text{for variations} \quad \delta\mathbf{u} = \partial_t\mathbf{v} + [\mathbf{u}, \mathbf{v}], \quad \delta\theta = -\mathbf{d}\theta \cdot \mathbf{v}, \tag{3.3}$$

where $\mathbf{v}(t, \mathbf{x})$ is an arbitrary vector field on $\mathcal{D}$ parallel to the boundary and with $\mathrm{div}(\bar\sigma\mathbf{v}) = 0$, (i.e., $\mathbf{v} \in \mathfrak{X}_{\bar\sigma\mu}(\mathcal{D})$ by Lemma 3.1), and with $\mathbf{v}(0, \mathbf{x}) = \mathbf{v}(T, \mathbf{x}) = 0$. The bracket $[\mathbf{u}, \mathbf{v}]$, locally given by $[\mathbf{u}, \mathbf{v}]^i := u^j\partial_j v^i - v^j\partial_j u^i$, is the Lie bracket of vector fields.

The expressions for $\delta\mathbf{u}$ and $\delta\theta$ in (3.3) follow by taking the variation of the first and second equalities in (3.2) and defining $\mathbf{v}(t, \mathbf{x})$ as $\mathbf{v}(t, \varphi(t, X)) = \delta\varphi(t, X)$. A direct and efficient way to obtain these expressions, or the variational principle (3.3), is to apply the general theory of Euler-Poincaré reduction on Lie groups, see [8].

In order to compute the associated equations, one needs to fix an appropriate space in nondegenerate duality with $\mathfrak{X}_{\bar\sigma\mu}(\mathcal{D})$. This is recalled in the next Lemma, which follows from the Hodge decomposition and shall play a crucial role in the discrete setting later. Recall that if V is a vector space, a space in nondegenerate duality with V is a vector space V' to together with a bilinear form $\langle\ ,\ \rangle : V' \times V \to \mathbb{R}$ such that $\langle\alpha, v\rangle = 0$, for all $v \in V$, implies $\alpha = 0$ and $\langle\alpha, v\rangle = 0$, for all $\alpha \in V'$, implies $v = 0$.

Lemma 3.2 *The space $\Omega^1(\mathcal{D})/\mathbf{d}\Omega^0(\mathcal{D})$ of one-forms modulo exact forms is in nondegenerate duality with the space $\mathfrak{X}_{\bar\sigma\mu}(\mathcal{D})$, the Lie algebra of $\mathrm{Diff}_{\bar\sigma\mu}(\mathcal{D})$. The nondegenerate duality pairing is given by*

$$\langle\ ,\ \rangle_{\bar\sigma} : \Omega^1(\mathcal{D})/\mathbf{d}\Omega^0(\mathcal{D}) \times \mathfrak{X}_{\bar\sigma\mu}(\mathcal{D}) \to \mathbb{R}, \quad \langle[\alpha], \mathbf{u}\rangle_{\bar\sigma} := \int_{\mathcal{D}} (\alpha \cdot \mathbf{u})\bar\sigma\mu, \tag{3.4}$$

where $[\alpha]$ denotes the equivalence class of α modulo exact forms.

Proof. It is well-known that if g is a Riemannian metric, with μ_g the associated volume form on $\mathcal{D}$, then

$$\langle\ ,\ \rangle : \Omega^1(\mathcal{D})/\mathbf{d}\Omega^0(\mathcal{D}) \times \mathfrak{X}_{\mu_g}(\mathcal{D}) \to \mathbb{R}, \quad \langle [\alpha], \mathbf{v}\rangle = \int_{\mathcal{D}} (\alpha \cdot \mathbf{v})\mu_g,$$

is a nondegenerate duality pairing, see e.g., [12, §14.1]. This result follows from the Hodge decomposition of 1-forms, which needs the introduction of a Riemannian metric g.

In our case, the volume forms μ and $\bar{\sigma}\mu$ are not necessarily associated to a Riemannian metric. We shall thus introduce a Riemannian metric g uniquely for the purpose of this proof, with associated Riemannian volume form μ_g. Let f be the function defined by $\bar{\sigma}\mu = f\mu_g$. Since $\mathcal{D}$ is orientable and connected, we have either $f > 0$ or $f < 0$ on $\mathcal{D}$. We can rewrite the duality pairing (3.4) as

$$\int_{\mathcal{D}} (\alpha \cdot \mathbf{u})\bar{\sigma}\mu = \int_{\mathcal{D}} (\alpha \cdot (f\mathbf{u}))\mu_g. \tag{3.5}$$

By successive applications of Lemma 3.1, we have

$$\operatorname{div}_{\mu_g}(f\mathbf{u}) = \operatorname{div}_{\frac{\bar{\sigma}}{f}\mu}(f\mathbf{u}) = f \operatorname{div}_{\bar{\sigma}\mu}(\mathbf{u}) = \frac{f}{\bar{\sigma}} \operatorname{div}_{\mu}(\bar{\sigma}\mathbf{u}) = 0,$$

where the last equality follows since $\mathbf{u} \in \mathfrak{X}_{\bar{\sigma}\mu}(\mathcal{D})$. This proves that $\mathbf{v} = f\mathbf{u} \in \mathfrak{X}_{\mu_g}(\mathcal{D})$. We can thus write the duality pairing $\langle\ ,\ \rangle_{\bar{\sigma}}$ in terms of the nondegenerate duality pairing (3.5) as $\langle [\alpha], \mathbf{u}\rangle_{\bar{\sigma}} = \langle [\alpha], f\mathbf{u}\rangle$, which proves that it is nondegenerate. ■

In a similar way to (3.4), we shall identify the dual to the space of functions $\mathcal{F}(\mathcal{D})$ with itself by using the nondegenerate duality pairing

$$\mathcal{F}(\mathcal{D}) \times \mathcal{F}(\mathcal{D}) \to \mathbb{R}, \quad \langle h, \theta\rangle_{\bar{\sigma}} = \int_{\mathcal{D}} (h\theta)\bar{\sigma}\mu. \tag{3.6}$$

Given a Lagrangian $\ell : \mathfrak{X}_{\bar{\sigma}\mu}(\mathcal{D}) \times \mathcal{F}(\mathcal{D}) \to \mathbb{R}$, the functional derivatives of ℓ are defined with respect to the parings (3.4) and (3.6) and denoted

$$\left[\frac{\delta \ell}{\delta \mathbf{u}}\right] \in \Omega^1(\mathcal{D})/\mathbf{d}\Omega^0(\mathcal{D}), \quad \text{for } \frac{\delta \ell}{\delta \mathbf{u}} \in \Omega^1(\mathcal{D}), \qquad \text{and} \qquad \frac{\delta \ell}{\delta \theta} \in \mathcal{F}(\mathcal{D}).$$

Proposition 3.3 *The variational principle (3.3) yields the partial differential equation*

$$\partial_t \frac{\delta \ell}{\delta \mathbf{u}} + \pounds_{\mathbf{u}} \frac{\delta \ell}{\delta \mathbf{u}} + \frac{\delta \ell}{\delta \theta} \mathbf{d}\theta = -\mathbf{d}p, \quad \textit{with} \quad \operatorname{div}_{\mu}(\bar{\sigma}\mathbf{u}) = 0, \ \ \mathbf{u} \parallel \partial\mathcal{D}, \tag{3.7}$$

where $\pounds_{\mathbf{u}}$ denotes the Lie derivative acting on one-forms, given by $\pounds_{\mathbf{u}}\alpha = \mathbf{d}(\mathbf{i}_{\mathbf{u}}\alpha) + \mathbf{i}_{\mathbf{u}}\mathbf{d}\alpha$. This equation is supplemented with the advection equation

$$\partial_t \theta + \mathbf{d}\theta \cdot \mathbf{u} = 0,$$

which follows from the definition of θ in (3.2).

Proof. By definition of the functional derivatives, we have

$$\delta \int_0^T \ell(\mathbf{u},\theta)dt = \int_0^T \int_{\mathcal{D}} \frac{\delta \ell}{\delta \mathbf{u}} \cdot \delta \mathbf{u}\, \bar{\sigma}\mu dt + \int_0^T \int_{\mathcal{D}} \frac{\delta \ell}{\delta \theta} \cdot \delta\theta\, \bar{\sigma}\mu dt.$$

Using the expression for $\delta\mathbf{u}$ in (3.3), integrating by parts, and using the equalities $\pounds_{\mathbf{u}}\mathbf{v} = [\mathbf{u},\mathbf{v}]$ and $\mathbf{d}(\alpha\cdot\mathbf{v})\cdot\mathbf{u} = (\pounds_{\mathbf{u}}\alpha)\cdot\mathbf{v} + \alpha\cdot(\pounds_{\mathbf{u}}\mathbf{v})$, the first term reads

$$-\int_0^T \int_{\mathcal{D}} \left(\partial_t \frac{\delta\ell}{\delta\mathbf{u}} + \pounds_{\mathbf{u}} \frac{\delta\ell}{\delta\mathbf{u}}\right)\cdot\mathbf{v}\bar{\sigma}\mu dt + \int_0^T \int_{\mathcal{D}} \mathbf{d}\left(\frac{\delta\ell}{\delta\mathbf{u}}\cdot\mathbf{v}\right)\cdot\mathbf{u}\bar{\sigma}\mu dt.$$

We can write $\mathbf{d}\left(\frac{\delta\ell}{\delta\mathbf{u}}\cdot\mathbf{v}\right)\cdot\mathbf{u} = \mathrm{div}_{\bar{\sigma}\mu}\left(\frac{\delta\ell}{\delta\mathbf{u}}\cdot\mathbf{v}\,\mathbf{u}\right) - \frac{\delta\ell}{\delta\mathbf{u}}\cdot\mathbf{v}\,\mathrm{div}_{\bar{\sigma}\mu}(\mathbf{u}) = \mathrm{div}_{\bar{\sigma}\mu}\left(\frac{\delta\ell}{\delta\mathbf{u}}\cdot\mathbf{v}\,\mathbf{u}\right)$, since $\mathrm{div}_{\bar{\sigma}\mu}(\mathbf{u}) = 0$. Then, by the Gauss Theorem,

$$\int_{\mathcal{D}} \mathrm{div}_{\bar{\sigma}\mu}\left(\frac{\delta\ell}{\delta\mathbf{u}}\cdot\mathbf{v}\,\mathbf{u}\right)\bar{\sigma}\mu = \int_{\partial\mathcal{D}} \frac{\delta\ell}{\delta\mathbf{u}}\cdot\mathbf{v}\,\mathbf{i}_{\mathbf{u}}\mu\,\bar{\sigma} = 0,$$

since $\mathbf{u} \parallel \partial\mathcal{D}$. Combining these results, we thus get

$$\int_0^T \int_{\mathcal{D}} \left(\partial_t \frac{\delta\ell}{\delta\mathbf{u}} + \pounds_{\mathbf{u}}\frac{\delta\ell}{\delta\mathbf{u}} + \frac{\delta\ell}{\delta\theta}\mathbf{d}\theta\right)\cdot\mathbf{v}\bar{\sigma}\mu dt = 0,$$

for all $\mathbf{v}\in\mathfrak{X}_{\bar{\sigma}\mu}(\mathcal{D})$. By Lemma 3.2, it follows that the one-form $\partial_t\frac{\delta\ell}{\delta\mathbf{u}} + \pounds_{\mathbf{u}}\frac{\delta\ell}{\delta\mathbf{u}} + \frac{\delta\ell}{\delta\theta}\mathbf{d}\theta$ is exact, i.e., there exists a function p such that this expression equals $\mathbf{d}p$. ■

Remark 3.4 We note that the statement of Proposition 3.3 does not need the introduction of a Riemannian metric g on $\mathcal{D}$. Only a volume form μ is fixed, together with a strictly positive function $\bar{\sigma}$. It can be however advantageous to formulate the equations (3.7) in terms of a Riemannian metric g (note that we do not suppose that μ or $\bar{\sigma}\mu$ equals μ_g). In this case, identifying one-forms and vector fields via the flat operator $\mathbf{u}\in\mathfrak{X}(\mathcal{D}) \to \mathbf{u}^\flat = g(\mathbf{u},_)\in\Omega^1(\mathcal{D})$, the space $\Omega^1(\mathcal{D})/\mathbf{d}\Omega^0(\mathcal{D})$ can be identified with the space of vector fields $\mathfrak{X}(\mathcal{D})$ modulo gradient (with respect to g) of functions. The nondegenerate duality pairing (3.4) thus reads

$$\langle[\mathbf{v}],\mathbf{u}\rangle_{\bar{\sigma}} = \int_{\mathcal{D}} g(\mathbf{v},\mathbf{u})\bar{\sigma}\mu. \tag{3.8}$$

In terms of this duality pairing, the equations (3.7) are equivalently written as

$$\partial_t\frac{\delta\ell}{\delta\mathbf{u}} + \mathbf{u}\cdot\nabla\frac{\delta\ell}{\delta\mathbf{u}} + \nabla\mathbf{u}^{\mathsf{T}}\cdot\frac{\delta\ell}{\delta\mathbf{u}} + \frac{\delta\ell}{\delta\theta}\nabla\theta = -\nabla p, \tag{3.9}$$

where ∇ acting on a vector field is the covariant derivative associated to the Riemannian metric g, ∇ acting on a function is the gradient relative to g, and $\nabla\mathbf{u}^{\mathsf{T}}$ denotes the transpose with respect to g.

We shall now apply this setting to the anelastic and the pseudo-incompressible equations. The fluid domain $\mathcal{D}$ is a subset of the vertical plane $\mathbb{R}^2 \ni (x,z)$ or of the space $\mathbb{R}^3\ni(x,y,z)$, and has a smooth boundary $\partial\mathcal{D}$. We fix a volume form μ on $\mathcal{D}$.

1) Anelastic equations. For the anelastic equation, we take $\bar{\sigma}(z) = \bar{\rho}(z)$, the reference mass density. The Lagrangian is given by

$$\ell(\mathbf{u}, \theta) = \int_{\mathcal{D}} \left(\frac{1}{2}|\mathbf{u}|^2 - c_p \bar{\pi}\theta \right) \bar{\rho}\mu, \quad \mathbf{u} \in \mathfrak{X}_{\bar{\rho}\mu}(\mathcal{D}), \tag{3.10}$$

where $\bar{\pi}(z)$ is such that $c_p \frac{\partial \bar{\pi}}{\partial z} = -\frac{g}{\bar{\theta}}$ and the norm is computed relative to the standard inner product on $\mathbb{R}^2$ or $\mathbb{R}^3$.

Relative to the pairings (3.8) and (3.6) we get

$$\frac{\delta \ell}{\delta \mathbf{u}} = \mathbf{u} \quad \text{and} \quad \frac{\delta \ell}{\delta \theta} = -c_p \bar{\pi}, \tag{3.11}$$

so that the Euler-Poincaré equations (3.9) read $\partial_t \mathbf{u} + \mathbf{u} \cdot \nabla \mathbf{u} + \nabla \mathbf{u}^\mathsf{T} \cdot \mathbf{u} - c_p \bar{\pi} \nabla \theta = -\nabla p$, in terms of the pressure p. To permit a comparison of these anelastic equations with those given in the standard form of (2.7) in terms of Exner pressure π', we note that $\nabla \mathbf{u}^\mathsf{T} \cdot \mathbf{u} = \frac{1}{2} \nabla |\mathbf{u}|^2$ and that $-c_p \bar{\pi} \nabla \theta$ differs from $-g \frac{\theta'}{\bar{\theta}} \mathbf{z}$ by a gradient term, indeed:

$$-c_p \bar{\pi} \nabla \theta = -c_p \nabla \left(\bar{\pi} \theta \right) + c_p (\nabla \bar{\pi}) \theta = -c_p \nabla \left(\bar{\pi} \theta \right) - g \frac{\theta}{\bar{\theta}} \mathbf{z} = -\nabla \left(c_p \bar{\pi} \theta + g z \right) - g \frac{\theta'}{\bar{\theta}} \mathbf{z}.$$

Therefore, with π' defined in terms of p by the equality $c_p \bar{\theta} \pi' = p + \frac{1}{2}|\mathbf{u}|^2 - g\mathbf{z} - c_p \bar{\pi} \theta$, the Euler-Poincaré equations yield the anelastic equations (2.7).

2) Pseudo-incompressible equations. In this case we take $\bar{\sigma}(z) := \bar{\rho}(z) \bar{\theta}(z)$ and the Lagrangian is given by

$$\ell(\mathbf{u}, \theta) = \int_{\mathcal{D}} \frac{1}{\theta} \left(\frac{1}{2}|\mathbf{u}|^2 - g z \right) \bar{\rho} \bar{\theta} \mu, \quad \mathbf{u} \in \mathfrak{X}_{\bar{\rho}\bar{\theta}\mu}(\mathcal{D}). \tag{3.12}$$

As before, the kinetic energy is computed relative to the standard inner product on $\mathbb{R}^2$ or $\mathbb{R}^3$. Relative to the pairings (3.8) and (3.6) we get

$$\frac{\delta \ell}{\delta \mathbf{u}} = \frac{1}{\theta} \mathbf{u} \quad \text{and} \quad \frac{\delta \ell}{\delta \theta} = -\frac{1}{\theta^2} \left(\frac{1}{2}|\mathbf{u}|^2 - g z \right), \tag{3.13}$$

so that the Euler-Poincaré equations (3.9) read

$$\partial_t \left(\frac{1}{\theta} \mathbf{u} \right) + \mathbf{u} \cdot \nabla \left(\frac{1}{\theta} \mathbf{u} \right) + \nabla \mathbf{u}^\mathsf{T} \cdot \frac{1}{\theta} \mathbf{u} - \frac{1}{\theta^2} \left(\frac{1}{2}|\mathbf{u}|^2 - g z \right) \nabla \theta = -\nabla p.$$

After some computations, using the relation $-\frac{g}{\bar{\theta}} = c_p \partial_z \bar{\pi}$, these equations recover the pseudo-incompressible system (2.8) with $c_p(\bar{\pi} + \pi') = p + \frac{1}{\theta}(\frac{1}{2}|\mathbf{u}|^2 - g z)$.

Based on these results, we can formulate the following statement that will allow us to derive the variational discretization of these two models by the discrete diffeomorphism group approach.

Theorem 3.5 *Consider a domain $\mathcal{D}$ with smooth boundary $\partial\mathcal{D}$ and volume form μ. The anelastic system with reference density $\bar{\rho}$, resp., the pseudo-incompressible system with reference density $\bar{\rho}$ and reference potential temperature $\bar{\theta}$ can be derived from an Euler-Poincaré variational principle for the Lie group*

$$G = \mathrm{Diff}_{\bar{\rho}\mu}(\mathcal{D}) \quad \textit{resp.} \quad G = \mathrm{Diff}_{\bar{\rho}\bar{\theta}\mu}(\mathcal{D}), \tag{3.14}$$

with Lagrangian (3.10), resp., (3.12).

Kelvin-Noether circulation theorems. The Euler-Poincaré formulation is well adapted for a systematic derivation of the circulation theorems, see [8]. From (3.7) one indeed deduces the following general form of the circulation theorem

$$\frac{d}{dt}\oint_{c_t}\frac{\delta \ell}{\delta \mathbf{u}} = -\oint_{c_t}\frac{\delta \ell}{\delta \theta}\mathbf{d}\theta, \tag{3.15}$$

where $c_t = \varphi(t, c_0)$ is a loop advected by the fluid flow $\varphi(t, _)$ and $\oint_{c_t}\alpha$ denotes the circulation of the one-form α along the loop c_t. Using the equation $\partial_t\theta + \mathbf{d}\theta\cdot\mathbf{u} = 0$, one also deduces another useful form, namely,

$$\frac{d}{dt}\oint_{c_t}\theta\frac{\delta \ell}{\delta \mathbf{u}} = -\oint_{c_t}\left(\theta\frac{\delta \ell}{\delta \theta}\mathbf{d}\theta - \theta\mathbf{d}p\right). \tag{3.16}$$

We shall not present the derivation of (3.15) and (3.16) since they follow from similar arguments with those explained in details in [8].

For the anelastic system, using (3.11) and the equalities $c_p\bar{\pi}\mathbf{d}\theta = c_p\mathbf{d}(\bar{\pi}\theta) - c_p\mathbf{d}\bar{\pi}\theta = c_p\mathbf{d}(\bar{\pi}\theta) + g\frac{\theta}{\bar{\theta}}\mathbf{z}$, expression (3.15) yields the equivalent forms

$$\frac{d}{dt}\oint_{c_t}\mathbf{u}\cdot d\mathbf{x} = c_p\oint_{c_t}\bar{\pi}\mathbf{d}\theta \qquad \text{or} \qquad \frac{d}{dt}\oint_{c_t}\mathbf{u}\cdot d\mathbf{x} = g\oint_{c_t}\frac{\theta}{\bar{\theta}}\mathbf{z}\cdot d\mathbf{x}$$

of the circulation theorem. For the pseudo-incompressible system, using (3.13) and the equalities $\frac{1}{\theta}\left(\frac{1}{2}|\mathbf{u}|^2 - gz\right)\mathbf{d}\theta - \theta\mathbf{d}p = \mathbf{d}\left(\frac{1}{2}|\mathbf{u}|^2 - gz\right) - c_p\mathbf{d}\pi\theta$, the expression (3.16) yields

$$\frac{d}{dt}\oint_{c_t}\mathbf{u}\cdot d\mathbf{x} = c_p\oint_{c_t}\pi\mathbf{d}\theta.$$

As shown further below, these conservation laws of the continuous equations, here presented with explicit formulas, are also preserved by the discrete variational discretizations that we will derive in the following section.

4 Variational discretizations

In this section we first quickly review from [14] the discrete diffeomorphism group approach in the incompressible case. Then, based on the results of Theorem 3.5, we show that an appropriate adaptation of this approach allows us to derive a variational discretization of the anelastic and pseudo-incompressible systems valid on a large class of mesh discretizations of the fluid domain.

Review of the discrete diffeomorphism group approach in the incompressible case. The spatial discretization of the equations is accomplished by considering the finite dimensional approximation of the group of volume preserving diffeomorphisms developed in [14], which we roughly recall below.

Given a mesh $\mathbb{M}$ on the fluid domain $\mathcal{D}$ with cells C_i, $i = 1, ..., N$, define a diagonal $N\times N$ matrix Ω consisting of cell volumes: $\Omega_i = \mathrm{Vol}(C_i)$. The discretization of the group $\mathrm{Diff}_\mu(\mathcal{D})$ of volume preserving diffeomorphisms of $\mathcal{D}$ is the matrix group

$$\mathsf{D}(\mathbb{M}) = \left\{q \in \mathrm{GL}(N)^+ \mid q\cdot\mathbf{1} = \mathbf{1} \ \text{ and } \ q^{\mathsf{T}}\Omega q = \Omega\right\}, \tag{4.1}$$

where $\mathrm{GL}(N)^+$ is the group of invertible $N \times N$ matrices with positive determinant, and $\mathbf{1}$ denotes the column $(1, ..., 1)^\mathsf{T}$ so that the first condition reads $\sum_{j=1}^N q_{ij} = 1$ for all $i = 1, ..., N$. The main idea behind this definition is the following (see [14] for the detailed treatment). Consider the linear action of $\mathrm{Diff}_\mu(\mathcal{D})$ on the space $\mathcal{F}(\mathcal{D})$ of functions on $\mathcal{D}$, given by

$$f \in \mathcal{F}(\mathcal{D}) \mapsto f \circ \varphi^{-1} \in \mathcal{F}(\mathcal{D}), \quad \varphi \in \mathrm{Diff}_\mu(\mathcal{D}). \tag{4.2}$$

This linear map has two key proporties:
(1) it preserves the L^2 inner product of functions;
(2) it preserves constant functions C on $\mathcal{D}$: $C \circ \varphi^{-1} = C$.
In the discrete setting, a function is discretized as a vector $F \in \mathbb{R}^N$ whose value F_i on cell C_i is regarded as the cell average of the function. Accordingly, the discrete L^2 inner product of two discrete functions is defined by

$$\langle F, G \rangle = F^\mathsf{T} \Omega G = \sum_{i=1}^N F_i \Omega_i G_i.$$

The discrete diffeomorphism group (4.1) is such that its action on discrete functions by matrix multiplication, is an approximation of the linear map (4.2). The conditions $q^\mathsf{T} \Omega q = \Omega$ and $q \cdot \mathbf{1} = \mathbf{1}$ are indeed the discrete analogues of the conditions (1) and (2) above, respectively.

The Lie algebra of $\mathsf{D}(\mathbb{M})$, denoted $\mathfrak{d}(\mathbb{M})$, is the space of Ω-antisymmetric, row-null matrices:

$$\mathfrak{d}(\mathbb{M}) = \{A \in \mathfrak{gl}(N) \mid A \cdot \mathbf{1} = 0 \ \text{ and } \ A^\mathsf{T} \Omega + \Omega A = 0\}.$$

The component A_{ij} of the matrix A is the weighted flux of the vector field $\mathbf{u}$ through the face common to the cells C_i and C_j. This relation induces a nonholonomic constraint on the Lie algebra $\mathfrak{d}(\mathbb{M})$ as only the fluxes through adjacent cells are non-zero:

$$\mathcal{S} = \{A \in \mathfrak{d}(\mathbb{M}) \mid A_{ij} \neq 0 \Rightarrow j \in N(i)\}, \tag{4.3}$$

in which $N(i)$ is the set of all indices of cells adjacent to cell C_i.

Once a discrete Lagrangian $\ell_d : \mathfrak{d}(\mathbb{M}) \to \mathbb{R}$ has been selected, the derivation of the spatial variational discretization then proceeds by applying an Euler-Poincaré variational principle to this Lagrangian that takes into account the nonholonomic constraint. This approach has been developed in [14] for the incompressible homogenous ideal fluid and extended to several models of incompressible fluids with advection equations in [7] and to rotating and/or stratified Boussinesq flows in [4].

Discrete diffeomorphism groups for the two models. The results obtained in Theorem 3.5 make it possible to extend this approach to treat the anelastic and pseudo-incompressible systems. The main idea consists in defining weighted versions of the volume of the cells in order to permit the use of the results recalled above in the incompressible case.

Given a mesh $\mathbb{M}$ on $\mathcal{D}$, a reference density $\bar{\rho}(z)$, and a reference potential temperature $\bar{\theta}(z)$ on $\mathcal{D}$, we define, respectively, the diagonal matrices $\Omega^{\bar{\rho}}$ and $\Omega^{\bar{\rho}\bar{\theta}}$ of $\bar{\rho}$-weighted and $\bar{\rho}\bar{\theta}$-weighted volumes as

$$\Omega_i^{\bar{\rho}} := \int_{C_i} \bar{\rho}(z) d\mathbf{x} \quad \text{and} \quad \Omega_i^{\bar{\rho}\bar{\theta}} := \int_{C_i} \bar{\rho}(z)\bar{\theta}(z) d\mathbf{x}.$$

The discrete versions of the diffeomorphism groups $\mathrm{Diff}_{\bar\rho\mu}(\mathcal{D})$ and $\mathrm{Diff}_{\bar\rho\bar\theta\mu}(\mathcal{D})$ in (3.14) are therefore

$$\mathsf{D}_{\bar\rho}(\mathbb{M}) := \big\{q \in \mathrm{GL}(N)^+ \mid q\cdot\mathbf{1}=\mathbf{1} \ \text{ and } \ q^{\mathsf{T}}\Omega^{\bar\rho}q=\Omega^{\bar\rho}\big\},$$
$$\mathsf{D}_{\bar\rho\bar\theta}(\mathbb{M}) := \big\{q \in \mathrm{GL}(N)^+ \mid q\cdot\mathbf{1}=\mathbf{1} \ \text{ and } \ q^{\mathsf{T}}\Omega^{\bar\rho\bar\theta}q=\Omega^{\bar\rho\bar\theta}\big\},$$

with Lie algebras

$$\mathfrak{d}_{\bar\rho}(\mathbb{M}) = \big\{A \in \mathfrak{gl}(N) \mid A\cdot\mathbf{1}=0 \ \text{ and } \ A^{\mathsf{T}}\Omega^{\bar\rho}+\Omega^{\bar\rho}A=0\big\},$$
$$\mathfrak{d}_{\bar\rho\bar\theta}(\mathbb{M}) = \big\{A \in \mathfrak{gl}(N) \mid A\cdot\mathbf{1}=0 \ \text{ and } \ A^{\mathsf{T}}\Omega^{\bar\rho\bar\theta}+\Omega^{\bar\rho\bar\theta}A=0\big\}.$$

In order to treat the anelastic and pseudo-incompressible cases, we also need to appropriately modify the relation between the components A_{ij} and the velocity vector fields $\mathbf{u}$, by taking into account the weights $\bar\rho$ and $\bar\theta$. For $\mathbf{u}\in\mathfrak{X}_{\bar\rho\mu}(\mathcal{D})$, resp., $\mathbf{u}\in\mathfrak{X}_{\bar\rho\bar\theta\mu}(\mathcal{D})$, we get

$$A_{ij} \simeq -\frac{1}{2\Omega_i^{\bar\rho}}\int_{D_{ij}}(\bar\rho\,\mathbf{u}\cdot\mathbf{n}_{ij})\mathrm{d}S, \quad \text{resp.,} \quad A_{ij} \simeq -\frac{1}{2\Omega_i^{\bar\rho\bar\theta}}\int_{D_{ij}}(\bar\rho\bar\theta\,\mathbf{u}\cdot\mathbf{n}_{ij})\mathrm{d}S, \tag{4.4}$$

in which D_{ij} is the boundary common to C_i and C_j, and $\mathbf{n}_{ij}$ is the normal vector field on D_{ij} pointing from C_i to C_j. The same nonholonomic constraint as before needs to be imposed, but this time on $\mathfrak{d}_{\bar\sigma}(\mathbb{M})$, namely,

$$\mathcal{S}_{\bar\sigma} = \{A\in\mathfrak{d}_{\bar\sigma}(\mathbb{M}) \mid A_{ij}\neq 0 \Rightarrow j\in N(i)\}. \tag{4.5}$$

This constraint induces a right-invariant linear constraint on the Lie group $\mathsf{D}_{\bar\sigma}(\mathbb{M})$: at $q\in\mathsf{D}_{\bar\sigma}(\mathbb{M})$, the constraint is defined as

$$\mathcal{S}_{\bar\sigma}(q) := \{\dot q\in T_q\mathsf{D}_{\bar\sigma}(\mathbb{M}) \mid \dot q q^{-1}\in\mathcal{S}_{\bar\sigma}\}\subset T_q\mathsf{D}_{\bar\sigma}(\mathbb{M}).$$

In addition to the matrix $A\in\mathfrak{d}_{\bar\sigma}(\mathbb{M})$ which discretizes the Eulerian velocity $\mathbf{u}$, we introduce the discrete potential temperature $\Theta\in\mathbb{R}^N$ whose component Θ_i is the average of the potential temperature θ on cell C_i.

Variational discretization for the two models. The variational discretization is carried out by mimicking the Euler-Poincaré approach of Theorem 3.5. Consider a discrete Lagrangian $L_{\Theta_0,d}: T\mathsf{D}_{\bar\sigma}(\mathbb{M})\to\mathbb{R}$ defined on the tangent bundle of the Lie group $\mathsf{D}_{\bar\sigma}(\mathbb{M})$ and being an approximation of the Lagrangian in (3.1). The parameter $\Theta_0\in\mathbb{R}^N$ is the discrete potential temperature in the Lagrangian description.

Hamilton's principle has to be appropriately modified to take into account the nonholonomic constraint, namely, we apply the Lagrange-d'Alembert principle stating that the action functional is critical with respect to variations subject to the constraint. In our case it reads

$$\delta\int_0^T L_{\Theta_0,d}(q,\dot q)dt = 0, \quad \text{for variations} \quad \delta q\in\mathcal{S}_{\bar\sigma}(q) \tag{4.6}$$

vanishing at $t=0,T$, and with $\dot q\in\mathcal{S}_{\bar\sigma}(q)$.

In a similar way with the continuous case, the relation between the Lagrangian variables $q(t)\in\mathsf{D}_{\bar\sigma}(\mathbb{M})$, $\Theta_0\in\mathbb{R}^N$, and the Eulerian variables $A(t)\in\mathfrak{d}_{\bar\sigma}(\mathbb{M})$, $\Theta(t)\in\mathbb{R}^N$, is given by the formulas

$$A(t) = \dot q(t)q(t)^{-1} \quad \text{and} \quad \Theta(t) = q(t)\Theta_0. \tag{4.7}$$

The discrete Lagrangian $L_{\Theta_0,d}$ is assumed to have the same right-invariance as its continuous counterpart in (3.1), hence it can be exclusively written in terms of the Eulerian variables in (4.7). We thus get the reduced Lagrangian

$$\ell_d = \ell_d(A,\Theta) : \mathfrak{d}_{\bar\sigma}(\mathbb{M}) \times \mathbb{R}^N \to \mathbb{R}.$$

The Eulerian version of the Lagrange-d'Alembert principle (4.6) is found to be

$$\delta \int_0^T \ell_d(A,\Theta)dt = 0, \quad \text{for variations} \quad \delta A = \partial_t Y + [Y,A], \quad \delta\Theta = Y\Theta, \tag{4.8}$$

in which $A \in \mathcal{S}_{\bar\sigma}$ and where Y is an arbitrary time dependent matrix in $\mathcal{S}_{\bar\sigma}$ vanishing at the endpoints. The expressions for the variations δA and $\delta\Theta$ in (4.8) are obtained by using the two relations (4.7). In particular, we have $Y = \delta q q^{-1}$, which is therefore an arbitrary time dependent matrix in $\mathcal{S}_{\bar\sigma}$ vanishing at $t = 0, T$. The principle (4.8) is a nonholonomic version of the Euler-Poincaré variational principle.

In order to derive the equations associated to the principle (4.8), we need to introduce appropriate dual spaces to the Lie algebra $\mathfrak{d}_{\bar\sigma}(\mathbb{M})$ and the space of discrete functions $\Omega^0_d(\mathbb{M}) = \mathbb{R}^N$. To this end, we recall from [7] that in the context of discrete diffeomorphism groups, a discrete one-form on $\mathbb{M}$ is identified with a skew-symmetric $N \times N$ matrix. The space of discrete one-forms is denoted by $\Omega^1_d(\mathbb{M})$. The discrete exterior derivative of a discrete function $F \in \Omega^0_d(\mathbb{M})$ is the discrete one-form $\mathrm{d}F$ given by

$$(\mathrm{d}F)_{ij} := F_i - F_j.$$

Then, given a strictly positive function $\bar\sigma(\mathbf{x}) > 0$, the discrete version of the L^2 pairing (3.4) is defined as

$$\langle\!\langle K, A \rangle\!\rangle_{\bar\sigma} := \mathrm{Tr}\left(K^\mathsf{T}\Omega^{\bar\sigma}A\right), \quad K \in \Omega^1_d(\mathbb{M}), \quad A \in \mathfrak{d}_{\bar\sigma}(\mathbb{M}). \tag{4.9}$$

By repeating the arguments of Theorem 2.4 of [7] for the discrete L^2 pairing (4.9) with weight $\bar\sigma$, we get the identification

$$\mathfrak{d}_{\bar\sigma}(\mathbb{M})^* \simeq \Omega^1_d(\mathbb{M})/\mathrm{d}\Omega^0_d(\mathbb{M}), \tag{4.10}$$

which is the discrete analogue of the identification in Lemma 3.2.

Concerning functions, the discrete analogue of the pairing (3.6) is given by

$$\langle F, G \rangle_{\bar\sigma} := F^\mathsf{T}\Omega^{\bar\sigma}G = \sum_{i=1}^N F_i\Omega^{\bar\sigma}_i G_i, \quad F, G \in \mathbb{R}^N. \tag{4.11}$$

A direct application of the principle (4.8) yields the following result.

Proposition 4.1 *A curve $(A(t),\Theta(t)) \in \mathfrak{d}_{\bar\sigma}(\mathbb{M}) \times \mathbb{R}^N$ is critical for the principle (4.8) if and only if there exists a discrete function $P \in \mathbb{R}^N$ such that the following equation holds*

$$\frac{d}{dt}\frac{\delta\ell_d}{\delta A_{ij}} + \left(\left[\frac{\delta\ell_d}{\delta A}\Omega^{\bar\sigma}, A\right](\Omega^{\bar\sigma})^{-1}\right)_{ij} - \frac{1}{2}\left(\frac{\delta\ell_d}{\delta\Theta_i} + \frac{\delta\ell_d}{\delta\Theta_j}\right)(\Theta_j - \Theta_i) + (P_i - P_j) = 0, \tag{4.12}$$

for all $j \in N(i)$, where the functional derivatives $\frac{\delta\ell_d}{\delta A}$ and $\frac{\delta\ell_d}{\delta\Theta}$ are computed with respect to the pairings (4.9) and (4.11).

Equation (4.12) yields a structure-preserving spatial discretization of the Euler-Poincaré equation (3.7) on the mesh $\mathbb{M}$. For the anelastic, resp., pseudo-incompressible equations, we will choose $\bar{\sigma} = \bar{\rho}$, resp., $\bar{\sigma} = \bar{\rho}\bar{\theta}$ and use in (4.12) suitable approximations

$$\ell_d = \ell_d(A, \Theta) : \mathfrak{d}_{\bar{\rho}}(\mathbb{M}) \times \mathbb{R}^N \to \mathbb{R}, \quad \text{resp.} \quad \ell_d = \ell_d(A, \Theta) : \mathfrak{d}_{\bar{\rho}\bar{\theta}}(\mathbb{M}) \times \mathbb{R}^N \to \mathbb{R}, \tag{4.13}$$

of the Lagrangians (3.10), resp., (3.12).

Anelastic system. The discrete Lagrangian associated to (3.10) is

$$\ell_d(A, \Theta) = \frac{1}{2} \left\langle\!\left\langle A^\flat, A \right\rangle\!\right\rangle_{\bar{\rho}} - c_p \left\langle \bar{\Pi}, \Theta \right\rangle_{\bar{\rho}} = \frac{1}{2} \sum_{ij} A^\flat_{ij} A_{ij} \Omega^{\bar{\rho}}_i - c_p \sum_i \bar{\Pi}_i \Theta_i \Omega^{\bar{\rho}}_i, \tag{4.14}$$

where the first, resp., the second duality pairing is given in (4.9), resp., (4.11), and $\bar{\Pi} \in \mathbb{R}^N$ is a discretization of the reference value $\bar{\pi}(z)$ of the Exner pressure. The first term in (4.14) is the discretization of the kinetic energy associated to a given Riemannian metric on $\mathcal{D}$ and is based on a suitable flat operator $A \in \mathcal{S}_{\bar{\rho}} \mapsto A^\flat \in \Omega^1_d(\mathbb{M})$ associated to the mesh $\mathbb{M}$, see [14].

The functional derivatives of ℓ_d with respect to the pairings $\langle\!\langle\, , \rangle\!\rangle_{\bar{\rho}}$ and $\langle\, , \rangle_{\bar{\rho}}$ are, respectively,

$$\frac{\delta \ell_d}{\delta A_{ij}} = A^\flat_{ij} \quad \text{and} \quad \frac{\delta \ell}{\delta \Theta_i} = -c_p \bar{\Pi}_i.$$

Using them in (4.12) with $\bar{\sigma} = \bar{\rho}$, we get the structure-preserving spatial discretization of the anelastic system on the mesh $\mathbb{M}$ as

$$\frac{d}{dt} A^\flat_{ij} + [A^\flat \Omega^{\bar{\rho}}, A]_{ij} \frac{1}{\Omega^{\bar{\rho}}_j} + c_p \frac{\bar{\Pi}_i + \bar{\Pi}_j}{2} (\Theta_j - \Theta_i) = -(P_i - P_j), \quad \text{for all } j \in N(i). \tag{4.15}$$

Pseudo-incompressible system. The discrete Lagrangian associated to (3.12) is

$$\ell_d(A, \Theta) = \frac{1}{2} \sum_{ij} \frac{1}{\Theta_i} A^\flat_{ij} A_{ij} \Omega^{\bar{\rho}\bar{\theta}}_i - g \sum_i \frac{1}{\Theta_i} Z_i \Omega^{\bar{\rho}\bar{\theta}}_i, \tag{4.16}$$

in which $Z \in \mathbb{R}^N$ is a discretization of the height z. Note that we are now using the volumes $\Omega^{\bar{\rho}\bar{\theta}}_i$.

The functional derivatives of ℓ_d with respect to the pairings $\langle\!\langle\, , \rangle\!\rangle_{\bar{\rho}\bar{\theta}}$ and $\langle\, , \rangle_{\bar{\rho}\bar{\theta}}$ are, respectively,

$$\frac{\delta \ell_d}{\delta A_{ij}} = \frac{1}{2} \left(\frac{1}{\Theta_i} + \frac{1}{\Theta_j} \right) A^\flat_{ij} =: M_{ij} \quad \text{and} \quad \frac{\delta \ell}{\delta \Theta_i} = \frac{1}{\Theta_i^2} \Big(g Z_i - k_i \Big), \quad k_i := \frac{1}{2} \sum_j A^\flat_{ij} A_{ij}.$$

Using them in (4.12) with $\bar{\sigma} = \bar{\rho}\bar{\theta}$, we get the structure-preserving spatial discretization of the pseudo-incompressible system on the mesh $\mathbb{M}$ as

$$\begin{aligned} \frac{d}{dt} M_{ij} + [M \Omega^{\bar{\rho}\bar{\theta}}, A]_{ij} \frac{1}{\Omega^{\bar{\rho}\bar{\theta}}_j} - \frac{1}{2} \Big(\frac{g Z_i - k_i}{\Theta_i^2} + \frac{g Z_j - k_j}{\Theta_j^2} \Big) (\Theta_j - \Theta_i) \\ = -(P_i - P_j), \quad \text{for all } j \in N(i). \end{aligned} \tag{4.17}$$

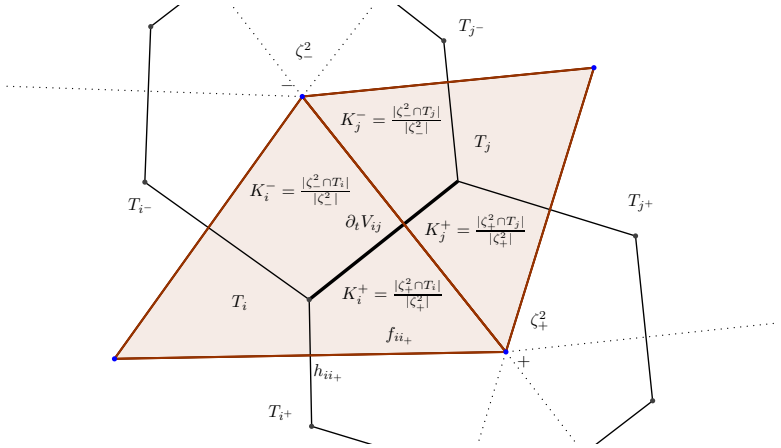

Figure 5.1: Notation and indexing conventions for the 2D simplicial mesh.

5 Numerical scheme on irregular simplicial meshes

In this section, we shall use the general results of §4, valid for any kind of reasonable (i.e. non-degenerated) meshes, to deduce the variational discretization on 2D simplicial meshes. On such meshes, we adopt the following notations (cf. Figure 5.1):

$$\begin{aligned} f_{ij} :=&\quad \text{length of the primal edge, located between triangle } i \text{ and triangle } j;\\ h_{ij} :=&\quad \text{length of the dual edge, between triangle } i \text{ and triangle } j;\\ \Omega_i :=&\quad \text{area of the primal simplex (triangle) } T_i. \end{aligned}$$

The flat operator on a 2D simplicial mesh is defined by the following two conditions, see [14],

$$\begin{aligned} &A^\flat_{ij} = 2\Omega_i \frac{h_{ij}}{f_{ij}} A_{ij}, \quad \text{for } j \in N(i),\\ &A^\flat_{ij} + A^\flat_{jk} + A^\flat_{ki} = K^e_j \left\langle \omega(A^\flat), \zeta^2_e \right\rangle, \quad \text{for } i,k \in N(j),\ k \notin N(i), \end{aligned} \tag{5.1}$$

in which e denotes the node common to triangles T_i, T_j, T_k and ζ^2_e denotes the dual cell to e. In (5.1), the vorticity $\omega(K)$ of a discrete one-form $K \in \Omega^1_d(\mathbb{M})$ is defined by

$$\left\langle \omega(K), \zeta^2_e \right\rangle := \sum_{\zeta^1_{mn} \in \partial\zeta^2_e} K_{mn},$$

where the sum is taken over the dual edges in the boundary $\partial\zeta^2_e$ counterclockwise around node e. The constant K^e_i is defined as

$$K^e_k := \frac{|\zeta^2_e \cap T_k|}{|\zeta^2_e|},$$

where $|\zeta^2_e|$ and $|\zeta^2_e \cap T_k|$ denote, respectively, the areas of ζ^2_e and $\zeta_e \cap T_k$. Note that the matrix $A^\flat$ defined in (5.1) is skew-symmetric, hence $A^\flat \in \Omega^1_d(\mathbb{M})$.

5.1 Boussinesq flow

Variational discretization of the Boussinesq fluid on regular Cartesian grids has been carried out in [4]. Here we shall derive from (4.12) the variational scheme on irregular 2D simplicial

grids. Recall that in this case $\mathrm{div}_\mu(\mathbf{u}) = 0$ and that the Boussinesq Lagrangian is given by

$$\ell(\mathbf{u}, b) = \int_{\mathcal{D}} \Big(\frac{1}{2}|\mathbf{u}|^2 + bz\Big)\mu.$$

The discrete Lagrangian is therefore chosen as $\ell_d : \mathfrak{d}(\mathbb{M}) \times \mathbb{R}^N \to \mathbb{R}$,

$$\ell_d(A, B) = \frac{1}{2}\left\langle\!\left\langle A^\flat, A \right\rangle\!\right\rangle + \langle B, Z\rangle\,,$$

where $B \in \mathbb{R}^N$ is the discrete buoyancy and Z is the discrete height function, i.e., Z_i denotes the z-coordinate of the center of cell C_i.

Using the Boussinesq Lagrangian and the flat operator (5.1), the discrete Euler-Poincaré equation (4.12) yields

$$\begin{cases} \partial_t A^\flat_{ij} + \left\langle \omega(A^\flat), \zeta^2_- \right\rangle \left(K^-_i A_{ii_-} + K^-_j A_{jj_-}\right) - \left\langle \omega(A^\flat), \zeta^2_+ \right\rangle \left(K^+_i A_{ii_+} + K^+_j A_{jj_+}\right) \\ \qquad\qquad = \dfrac{Z_i + Z_j}{2}(B_j - B_i) + (\tilde{P}_j - \tilde{P}_i), \quad \text{for all } j \in N(i), \\ \partial_t B_i - \displaystyle\sum_{j \in N(i)} A_{ij} B_j = 0, \end{cases} \tag{5.2}$$

where $\Omega_i A_{ij} = -\Omega_j A_{ji}$, for all i, j, and $\sum_{j\in N(i)} A_{ij} = 0$, for all i, and where $\tilde{P}$ is related to P in (4.12) via

$$\tilde{P}_i = P_i + \sum_{k \in N(i)} A^\flat_{ik} A_{ik}. \tag{5.3}$$

We note that the momentum equation (5.2) corresponds to the discretization of the following form of the Boussinesq equation:

$$\partial_t \mathbf{u}^\flat + \mathbf{i_u} \mathbf{d}\mathbf{u}^\flat = -z\mathbf{d}b - \mathbf{d}\tilde{p}, \tag{5.4}$$

where, similarly to (5.3), $\tilde{p} = \mathbf{i_u}\mathbf{u}^\flat + p$, with p the pressure function arising in the Euler-Poincaré formulation (3.7). The form (5.4) is easily seen to be equivalent to the standard form (2.4) with $P_\mathrm{b} = zb + p + \frac{1}{2}|\mathbf{u}|^2 = zb + \tilde{p} - \frac{1}{2}|\mathbf{u}|^2$.

Recall that the Lie algebra element $A \in \mathfrak{d}(\mathbb{M})$ and the velocity $\mathbf{u}$ are related as

$$A_{ij} \simeq -\frac{1}{2\Omega_i} \int_{f_{ij}} (\mathbf{u} \cdot \mathbf{n}) \mathrm{d}S.$$

We introduce the discrete velocity V_{ij} such that $A_{ij} = -\frac{1}{2\Omega_i} f_{ij} V_{ij}$. We thus get $A^\flat_{ij} = -h_{ij} V_{ij}$ for $i \in N(j)$ and the semidiscrete Boussinesq momentum equation (5.2) becomes

$$\partial_t V_{ij} + \mathrm{Adv}_\mathrm{b}(V)_{ij} = \mathrm{F}_\mathrm{b}(B)_{ij} - (\nabla_\mathrm{b} \tilde{P})_{ij}, \tag{5.5}$$

where we defined

$$\begin{aligned}
\mathrm{Adv_b}(V)_{ij} &:= -\frac{1}{h_{ij}|\zeta^2_-|}\Big(\sum_{\zeta^1_{mn}\in\partial\zeta^2_-} h_{mn}V_{mn}\Big)\left(\frac{|\zeta^2_-\cap T_i|}{2\Omega_i}f_{ii_-}V_{ii_-}+\frac{|\zeta^2_-\cap T_j|}{2\Omega_j}f_{jj_-}V_{jj_-}\right)\\
&\quad+\frac{1}{h_{ij}|\zeta^2_+|}\Big(\sum_{\zeta^1_{mn}\in\partial\zeta^2_+} h_{mn}V_{mn}\Big)\left(\frac{|\zeta^2_+\cap T_i|}{2\Omega_i}f_{ii_+}V_{ii_+}+\frac{|\zeta^2_+\cap T_j|}{2\Omega_j}f_{jj_+}V_{jj_+}\right),\\
\mathrm{F_b}(B)_{ij} &:= -\frac{Z_i+Z_j}{2h_{ij}}(B_j-B_i),\\
(\nabla_{\mathrm{b}}\tilde{P})_{ij} &:= \frac{1}{h_{ij}}(\tilde{P}_j-\tilde{P}_i).
\end{aligned}$$

We note that since $A\cdot\mathbf{1}=0$, we get $\sum_{j\in N(i)} f_{ij}V_{ij}=0$, which corresponds to the divergence free condition. We used everywhere the index b, referring to Boussinesq, to distinguish from the expressions occurring further below for the other two models.

5.2 Anelastic flow

The anelastic Lagrangian is given in (3.10) and the discrete Lagrangian $\ell_d : \mathfrak{d}_{\bar\rho}(\mathbb{M})\times\mathbb{R}^N\to\mathbb{R}$ in (4.14). Recall that in this case $\mathrm{div}_\mu(\bar\rho\mathbf{u})=0$. The flat operator (5.1) has to be slightly modified in order to produce a skew-symmetric matrix, namely, we modify the first line in (5.1) to

$$A^\flat := M^{(A)}, \quad \text{for the matrix } M \text{ defined by } \; M_{ij} := 2\Omega_i\frac{h_{ij}}{f_{ij}}A_{ij}, \tag{5.6}$$

in which $(\cdot)^{(A)}$ denotes the skew-symmetric part. For the Boussinesq model, this definition recovers (5.1), since the matrix M is in this case already skew-symmetric. One checks that this definition still satisfies the properties of a flat operator in [14].

The general discrete anelastic equations (4.15) yield

$$\begin{cases}
\partial_t A^\flat_{ij}+\big\langle\omega(A^\flat),\zeta^2_-\big\rangle\big(K^-_iA_{ii_-}+K^-_jA_{jj_-}\big)-\big\langle\omega(A^\flat),\zeta^2_+\big\rangle\big(K^+_iA_{ii_+}+K^+_jA_{jj_+}\big)\\
\qquad\qquad=-c_p\dfrac{\bar\Pi_i+\bar\Pi_j}{2}(\Theta_j-\Theta_i)+(\tilde P_j-\tilde P_i),\quad \text{for all } j\in N(i),\\
\partial_t\Theta_i-\displaystyle\sum_{j\in N(i)}A_{ij}\Theta_j=0,
\end{cases} \tag{5.7}$$

where $\Omega^{\bar\rho}_iA_{ij}=-\Omega^{\bar\rho}_jA_{ji}$, for all i,j, and $\sum_{j\in N(i)}A_{ij}=0$, for all i, and where $\tilde P$ is related to P in (4.12) and (4.15) as before via the formula (5.3). We note that the momentum equation (5.7) corresponds to the discretization of the following form of the anelastic equation:

$$\partial_t\mathbf{u}^\flat+\mathbf{i_u}\mathbf{d}\mathbf{u}^\flat=c_p\bar\pi\mathbf{d}\theta-\mathbf{d}\tilde p, \tag{5.8}$$

where, similarly to (5.3), $\tilde p=\mathbf{i_u}\mathbf{u}^\flat+p$, with p the pressure function arising in the Euler-Poincaré formulation (3.7). The form (5.8) was shown in §3 to be equivalent to the standard form (2.6).

Recall that the Lie algebra element $A\in\mathfrak{d}_{\bar\rho}(\mathbb{M})$ and the velocity $\mathbf{u}$ are related as

$$A_{ij}\simeq-\frac{1}{2\Omega^{\bar\rho}_i}\int_{f_{ij}}(\bar\rho\,\mathbf{u}\cdot\mathbf{n})\mathrm{d}S.$$

We thus introduce the velocity V_{ij} such that $A_{ij} = -\frac{1}{2\Omega_i^{\bar\rho}} f_{ij}\bar\rho_{ij}V_{ij}$, in which $\bar\rho_{ij} := \frac{\bar\rho_i+\bar\rho_j}{2}$, with $\bar\rho_i := \Omega_i^{\bar\rho}/\Omega_i$ the mean value of $\bar\rho(z)$ over cell C_i. We get the relation $A_{ij}^\flat = -h_{ij}\sigma_{ij}^{\mathrm{a}}V_{ij}$, where $\sigma_{ij}^{\mathrm{a}} := \frac{\bar\rho_{ij}}{2}\left(\frac{1}{\bar\rho_i}+\frac{1}{\bar\rho_j}\right)$. In terms of V, the semidiscrete anelastic momentum equation (5.7) becomes

$$\partial_t V_{ij} + \mathrm{Adv}_{\mathrm{a}}(V)_{ij} = \mathrm{F}_{\mathrm{b}}(\Theta)_{ij} - (\nabla_{\mathrm{a}}\tilde P)_{ij}, \tag{5.9}$$

where we defined

$$\begin{aligned}
&\mathrm{Adv}_{\mathrm{a}}(V)_{ij} :=\\
&-\frac{1}{\sigma_{ij}^{\mathrm{a}}h_{ij}|\zeta_-^2|}\Big(\sum_{\zeta^1_{mn}\in\partial\zeta^2_-}\sigma^{\mathrm{a}}_{mn}h_{mn}V_{mn}\Big)\left(\frac{|\zeta_-^2\cap T_i|}{2\Omega_i\bar\rho_i}f_{ii_-}\bar\rho_{ii_-}V_{ii_-}+\frac{|\zeta_-^2\cap T_j|}{2\Omega_j\bar\rho_j}f_{jj_-}\bar\rho_{jj_-}V_{jj_-}\right)\\
&+\frac{1}{\sigma_{ij}^{\mathrm{a}}h_{ij}|\zeta_+^2|}\Big(\sum_{\zeta^1_{mn}\in\partial\zeta^2_+}\sigma^{\mathrm{a}}_{mn}h_{mn}V_{mn}\Big)\left(\frac{|\zeta_+^2\cap T_i|}{2\Omega_i\bar\rho_i}f_{ii_+}\bar\rho_{ii_+}V_{ii_+}+\frac{|\zeta_+^2\cap T_j|}{2\Omega_j\bar\rho_j}f_{jj_+}\bar\rho_{jj_+}V_{jj_+}\right),\\
&\mathrm{F}_{\mathrm{a}}(\Theta)_{ij} := \frac{c_p}{\sigma_{ij}^{\mathrm{a}}h_{ij}}\frac{\bar\Pi_i+\bar\Pi_j}{2}(\Theta_j-\Theta_i),\\
&(\nabla_{\mathrm{a}}\tilde P)_{ij} := \frac{1}{\sigma_{ij}^{\mathrm{a}}h_{ij}}(\tilde P_j-\tilde P_i).
\end{aligned}$$

5.3 Pseudo-incompressible flow

The pseudo-incompressible Lagrangian is given in (3.12) and the discrete Lagrangian $\ell_d : \mathfrak{d}_{\bar\rho}(\mathbb{M})\times\mathbb{R}^N\to\mathbb{R}$ is given in (4.16). Recall that in this case $\mathrm{div}_\mu(\bar\rho\bar\theta\mathbf{u}) = 0$. We take the flat operator (5.1) with the first line modified as in (5.6)

The general discrete pseudo-incompressible equations (4.17) yield

$$\begin{cases}
\partial_t M_{ij} + \langle\omega(M),\zeta_-^2\rangle\left(K_i^-A_{ii_-}+K_j^-A_{jj_-}\right) - \langle\omega(M),\zeta_+^2\rangle\left(K_i^+A_{ii_+}+K_j^+A_{jj_+}\right)\\
\qquad\qquad = \frac{1}{2}\left(\frac{gZ_i-k_i}{\Theta_i^2}+\frac{gZ_j-k_j}{\Theta_j^2}\right)(\Theta_j-\Theta_i)+(\tilde P_j-\tilde P_i), \quad \text{for all } j\in N(i),\\
M_{ij} = \frac{1}{2}\left(\frac{1}{\Theta_i}+\frac{1}{\Theta_j}\right)A_{ij}^\flat,\\
\partial_t\Theta_i - \sum_{j\in N(i)}A_{ij}\Theta_j = 0,
\end{cases} \tag{5.10}$$

where $\Omega_i^{\bar\rho\bar\theta}A_{ij} = -\Omega_j^{\bar\rho\bar\theta}A_{ji}$, for all i,j, and $\sum_{\in N(i)}A_{ij}=0$, for all i, and where $\tilde P$ is related to P in (4.12) and (4.17) by the fomula

$$\tilde P_i = P_i + \sum_{k\in N(i)} M_{ik}A_{ik}. \tag{5.11}$$

We note that the momentum equation (5.10) corresponds to the discretization of the following form of the pseudo-incompressible equation:

$$\partial_t\left(\frac{1}{\theta}\mathbf{u}^\flat\right) + \frac{1}{\theta}\mathbf{i}_{\mathbf{u}}\mathbf{d}\mathbf{u}^\flat = -\frac{1}{\theta^2}(gz-\frac{1}{2}|\mathbf{u}|^2)\mathbf{d}\theta - \mathbf{d}\tilde p, \tag{5.12}$$

where, similarly to (5.11), $\tilde{p} = \frac{1}{\theta}\mathbf{i}_{\mathbf{u}}\mathbf{u}^\flat + p$, with p the pressure function arising in the Euler-Poincaré formulation (3.7). The form (5.12) was shown in §3 to be equivalent to the standard form (2.8).

Recall that the Lie algebra element $A \in \mathfrak{d}_{\bar{\rho}\bar{\theta}}(\mathbb{M})$ and the velocity $\mathbf{u}$ are related as

$$A_{ij} \simeq -\frac{1}{2\Omega_i^{\bar{\rho}\bar{\theta}}} \int_{f_{ij}} (\bar{\rho}\bar{\theta}\,\mathbf{u}\cdot\mathbf{n})\mathrm{d}S.$$

We thus introduce the velocity V_{ij} such that $A_{ij} = -\frac{1}{2\Omega_i^{\bar{\rho}\bar{\theta}}} f_{ij}\overline{\rho\theta}_{ij}V_{ij}$, in which $\overline{\rho\theta}_{ij} := \frac{\overline{\rho\theta}_i + \overline{\rho\theta}_j}{2}$, with $\overline{\rho\theta}_i := \Omega_i^{\bar{\rho}\bar{\theta}}/\Omega_i$ the mean value of $\bar{\rho}(z)\bar{\theta}(z)$ over cell C_i. We get the relation $A_{ij}^\flat = -h_{ij}\sigma_{ij}^{\mathrm{pi}}V_{ij}$, where $\sigma_{ij}^{\mathrm{pi}} := \frac{\overline{\rho\theta}_{ij}}{2}\left(\frac{1}{\overline{\rho\theta}_i} + \frac{1}{\overline{\rho\theta}_j}\right)$. In terms of V, the semidiscrete pseudo-incompressible momentum equation (5.10) becomes

$$\partial_t(\widetilde{\Theta}_{ij}V_{ij}) + \mathrm{Adv}_{\mathrm{pi}}(V,\Theta)_{ij} = \mathrm{F}_{\mathrm{pi}}(\Theta)_{ij} - (\nabla_{\mathrm{pi}}\tilde{P})_{ij}, \tag{5.13}$$

where we defined

$$\begin{aligned}
&\mathrm{Adv}_{\mathrm{pi}}(V,\Theta)_{ij} := \\
&-\frac{1}{\sigma_{ij}^{\mathrm{pi}}h_{ij}|\zeta_-^2|}\Big(\sum_{\zeta_{mn}^1\in\partial\zeta_-^2}\sigma_{mn}^{\mathrm{pi}}h_{mn}\widetilde{\Theta}_{mn}V_{mn}\Big)\left(\frac{|\zeta_-^2\cap T_i|}{2\Omega_i\overline{\rho\theta}_i}f_{ii_-}\overline{\rho\theta}_{ii_-}V_{ii_-} + \frac{|\zeta_-^2\cap T_j|}{2\Omega_j\overline{\rho\theta}_j}f_{jj_-}\overline{\rho\theta}_{jj_-}V_{jj_-}\right)\\
&+\frac{1}{\sigma_{ij}^{\mathrm{pi}}h_{ij}|\zeta_+^2|}\Big(\sum_{\zeta_{mn}^1\in\partial\zeta_+^2}\sigma_{mn}^{\mathrm{pi}}h_{mn}\widetilde{\Theta}_{mn}V_{mn}\Big)\left(\frac{|\zeta_+^2\cap T_i|}{2\Omega_i\overline{\rho\theta}_i}f_{ii_+}\overline{\rho\theta}_{ii_+}V_{ii_+} + \frac{|\zeta_+^2\cap T_j|}{2\Omega_j\overline{\rho\theta}_j}f_{jj_+}\overline{\rho\theta}_{jj_+}V_{jj_+}\right),\\
&\mathrm{F}_{\mathrm{pi}}(V,\Theta)_{ij} := -\frac{1}{2\sigma^{\mathrm{pi}}h_{ij}}\left(\frac{gZ_i-k_i}{\Theta_i^2} + \frac{gZ_j-k_j}{\Theta_j^2}\right)(\Theta_j-\Theta_i),\\
&(\nabla_{\mathrm{a}}\tilde{P})_{ij} := \frac{1}{\sigma_{ij}^{\mathrm{pi}}h_{ij}}(\tilde{P}_j - \tilde{P}_i).
\end{aligned}$$

5.4 Time integration and Poisson solvers

Since the spatial discretization has be realized in a structure-preserving way, a corresponding temporal variational discretization follows by applying the general discrete (in time) Euler-Poincaré approach, as it has be done in [7], [4] to which we refer for a detailed treatment. Hence, the temporal scheme consists of the following two steps.

Given the time t and a time step size Δt, we first compute $\Theta^{t+1} = \tau(hA^t)\Theta^t$ (with $\Theta = B$ in case of Boussinesq), in which τ is the Cayley transform. To this end we represent τ by the equation:

$$(I - \frac{1}{2}\Delta t A^t)\Theta^{t+1} = (I + \frac{1}{2}\Delta t A^t)\Theta^t. \tag{5.14}$$

with I the identity matrix (cf. [4] for more details). In the second step, the following update equations are solved. They are given in explicit form for the Boussinesq/anelastic schemes by

$$\frac{V_{ij}^{t+1} - V_{ij}^t}{\Delta t} = -\frac{1}{2}\,\mathrm{Adv}_{\mathrm{b/a}}(V^{t+1})_{ij} - \frac{1}{2}\,\mathrm{Adv}_{\mathrm{b/a}}(V^t)_{ij} - \mathrm{F}_{\mathrm{b/a}}(\Theta^{t+1})_{ij} - (\nabla_{\mathrm{b/a}}\tilde{P}^{t+1})_{ij}\ , \tag{5.15}$$

and for the pseudo-incompressible equation by

$$\frac{\widetilde{\Theta}_{ij}^{t+1}V_{ij}^{t+1} - \widetilde{\Theta}_{ij}^{t}V_{ij}^{t}}{\Delta t} = -\frac{1}{2}\,\mathrm{Adv}_{\mathrm{pi}}(V^{t+1},\Theta^{t+1}) - \frac{1}{2}\,\mathrm{Adv}_{\mathrm{pi}}(V^{t},\Theta^{t})_{ij} \\ - \mathrm{F}_{\mathrm{pi}}(V^{t},\Theta^{t+1})_{ij} - (\nabla_{\mathrm{pi}}\tilde{P}^{t+1})_{ij}\ . \tag{5.16}$$

This time update scheme, derived from discrete Euler-Poincaré equations, is analogous to a Crank-Nicolson time update scheme. To solve these implicit equations, we proceed as follows. Noting that Θ^{t+1} has been calculated first and is thus known, we rearrange the equations into known and unknown parts as

$$V_{ij}^{t+1} = \underbrace{V_{ij}^{t} - \frac{\Delta t}{2}\,\mathrm{Adv}_{\mathrm{b/a}}(V^{t})_{ij} - \Delta t\,\mathrm{F}_{\mathrm{b/a}}(\Theta^{t+1})_{ij}}_{=:\mathrm{G}_{\mathrm{b/a}}(V^{t})_{ij}} - \frac{\Delta t}{2}\,\mathrm{Adv}_{\mathrm{b/a}}(V^{t+1})_{ij} \\ - \Delta t(\nabla_{\mathrm{b/a}}P^{t+1})_{ij}\,, \tag{5.17}$$

and similarly for the pseudo-incompressible equations:

$$V_{ij}^{t+1} = \underbrace{\frac{\widetilde{\Theta}^{t}}{\widetilde{\Theta}^{t+1}}V_{ij}^{t} - \frac{\Delta t}{2\widetilde{\Theta}^{t+1}}\,\mathrm{Adv}_{\mathrm{pi}}(V^{t},\Theta^{t})_{ij} - \frac{\Delta t}{\widetilde{\Theta}^{t+1}}\,\mathrm{F}_{\mathrm{pi}}(V^{t},\Theta^{t+1})_{ij}}_{=:\mathrm{G}_{\mathrm{pi}}(V^{t})_{ij}} \\ - \frac{\Delta t}{2\widetilde{\Theta}^{t+1}}\,\mathrm{Adv}_{\mathrm{pi}}(V^{t+1},\Theta^{t+1})_{ij} - \frac{\Delta t}{\widetilde{\Theta}^{t+1}}(\nabla_{\mathrm{pi}}P^{t+1})_{ij}\ . \tag{5.18}$$

We can summaries the edge values into vector arrays, which we will indicate by omitting the notation ij. Then, we solve these vector equations for Boussinesq, anelasic, and pseudo-incompressible schemes by a *fixed point iteration*, given by the following algorithm:

1. Start loop over $k = 0$ with initial guess at t: $V_{k=0}^{*} = V^{t}$ and $P_{k=0}^{*} = 0$
2. Calculate tentative velocity $\widetilde{V}_{k}^{*}$:
   - Boussinesq/anelastic: $\widetilde{V}_{k}^{*} = \mathrm{G}_{\mathrm{b/a}}(V^{t}) - \frac{\Delta t}{2}\,\mathrm{Adv}_{\mathrm{b/a}}(V_{k}^{*})$;
   - Pseudo-incompressible: $\widetilde{V}_{k}^{*} = \mathrm{G}_{\mathrm{pi}}(V^{t}) - \frac{\Delta t}{2\widetilde{\Theta}^{t+1}}\,\mathrm{Adv}_{\mathrm{pi}}(V_{k}^{*},\Theta^{t+1})$;
3. Calculate pressure P_{k+1}^{*} by solving the Poisson equation:
   - Boussinesq ($\widehat{\rho} = 1$)/anelastic ($\widehat{\rho} = \bar{\rho}$): $\nabla\cdot\left(\widehat{\rho}\,\nabla_{\mathrm{b/a}}P_{k+1}^{*}\right) = \frac{1}{\Delta t}\nabla\cdot(\widehat{\rho}\,\widetilde{V}_{k}^{*})$;
   - Pseudo-incompressible: $\nabla\cdot\left(\frac{\bar{\rho}\bar{\Theta}}{\widetilde{\Theta}^{t+1}}\nabla_{\mathrm{pi}}P_{k+1}^{*}\right) = \frac{1}{\Delta t}\nabla\cdot(\bar{\rho}\bar{\Theta}\widetilde{V}_{k}^{*})$;
4. Update velocity and set $k + 1 = k$:
   - Boussinesq/anelastic: $V_{k+1}^{*} = \widetilde{V}_{k}^{*} - \Delta t\nabla_{\mathrm{b/a}}P_{k+1}^{*}$;
   - Pseudo-incompressible: $V_{k+1}^{*} = \widetilde{V}_{k}^{*} - \frac{\Delta t}{\widetilde{\Theta}^{t+1}}\nabla_{\mathrm{pi}}P_{k+1}^{*}$;

5. Stop loop over k if $||V^*_{k+1} - V^*_k|| < \epsilon$ for a small positive ϵ.

Substituting the tentative velocity $\widetilde{V}^*_k$ into the velocity update equation (step 4), we realize that in case of convergence, i.e. $V^*_{k+1} \to V^{t+1}$ and $P^*_{k+1} \to P^{t+1}$, this algorithm indeed solves equations (5.17) and (5.18).

Please note that the Poisson equations result from multiplying the anelastic momentum equations by $\bar{\rho}$ and the pseudo-incompressible by $\bar{\rho}\bar{\Theta}$ while imposing $\nabla \cdot (\bar{\rho} V^{t+1}) = 0$ or $\nabla \cdot \left(\bar{\rho}\bar{\Theta} V^{t+1}\right) = 0$, respectively. In the latter case we additionally assumed $\widetilde{\Theta}^* = \widetilde{\Theta}^{k+1}$. The respective divergence operators, denoted as $\nabla \cdot (\widehat{\rho} V) = \sum_{j \in N(i)} \frac{\widehat{\rho}_{ij} h_{ij} V_{ij}}{\Omega_i} = 0$, with $\widehat{\rho}_{ij} = 1$, $\widehat{\rho}_{ij} = \bar{\rho}_{ij}$, and $\widehat{\rho}_{ij} = (\bar{\rho}\bar{\Theta})_{ij}$, for the Boussinesq, anelastic, and pseudo-incompressible schemes, respectively, follow directly from the corresponding definitions of A and the divergence-freeness constraint $\sum_{j \in N(i)} A_{ij} = 0$, for all i.

Being derived both spatially and temporally via the Euler-Poincaré approach, the schemes (5.15) and (5.16) admit discrete version of the Kelvin circulation theorem. We refer to [7] and [4] for detailed discussions of the discrete Kelvin circulation theorems and its application to several examples. Since the application to the present models is similar we shall not repeat it here.

6 Numerical tests

We study numerically the behavior of the variational discretization schemes for the Boussinesq, anelastic, and pseudo-incompressible equations for regular and irregular computational meshes. On various test cases we investigate the models' dynamical behavior and their conservation of mass and energy. Descending from variational principles, these schemes are supposed to conserve the latter quantities to a high degree. Moreover as these models support internal gravity waves, we are interested in a quantitative evaluation of their discrete dispersion relations.

For all ensuing test cases we perform the simulations on regular and irregular triangular meshes. The regular meshes consist of equilateral triangles of constant edge length $f = |f_{ij}|$, where $f_{ij}, j = 1, 2, 3$, denote the edges of triangle T_i (cf. notation of Section 5). The distance between neighboring vertices in x-direction is given by $f_x := f$ while the height of the triangles in z-direction is given by $f_z := \frac{\sqrt{3}}{2} f$. Given a domain size of $L_x \times L_z$, in which L_x and L_z denote the domain's length in x- and z-directions, respectively, the *mesh resolution*, denoted by $2 \cdot N_x \times N_z$ for $N_x := L_x/f_x$ and $N_y := L_z/f_z$, corresponds to the number of triangular cells.

To construct irregular meshes, we start from a regular one and randomly move the regularly distributed *internal* vertices – i.e. vertices that do *not* belong to boundary cells – from point $\mathbf{x_i} = (x_i, z_i)$ to $\mathbf{x_i} + \delta\mathbf{x_i}$ within the bounds $|\delta x_i| < c \cdot f_x \cdot r$ and $|\delta z_i| < c \cdot f_z \cdot r$, for a positive constant c and some random number $r \in [-0.5, 0.5]$. Leaving the boundary triangles regular is not necessary in terms of the discretization schemes, however it eases the way of how we implemented the boundary conditions (a more general treatment is possible, but we leave it to future work).

For our studies we use (i) $c = 0.1$ and (ii) $c = 0.2$ to construct meshes with different degrees of irregularity. The resulting distortion of the meshes can be quantified using a grid quality measure introduced in [2] that measures the distortion of the dual cells: $\Delta h(\mathbf{x}) := \frac{\max_j \ h_{ij}}{\min_j \ h_{ij}}$, in which h_{ij} is the length of dual edge j of dual cell ζ^2_i that contains point $\mathbf{x}$. High values of Δh indicate strongly deformed cells. As such cells may impact on the quality of the simulations, as

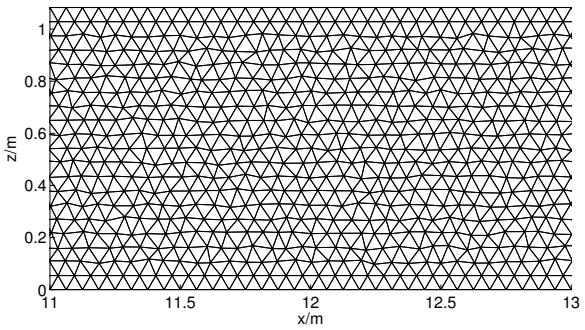

Figure 6.1: Section of central part of irregular mesh (ii) with $\max_{\mathbf{x}\in\Omega} \Delta h(\mathbf{x}) \leq 7$ for a resolution of $2 \cdot 384 \times 20$ triangular cells.

shown in [2], we apply for the advection dominated test cases in Section 6.2 the irregular mesh (i), where we restrict the irregularity of the grid to $\max_{\mathbf{x}\in\Omega} \Delta h(\mathbf{x}) \leq 1.5$ by setting $c = 0.1$. In contrast to such rather smooth grid, we apply for the hydrostatic adjustment test cases in Section 6.1 the irregular mesh (ii) for $c = 0.2$ with $\max_{\mathbf{x}\in\Omega} \Delta h(\mathbf{x}) \leq 7$ (cf. Figure 6.1) in order to illustrate that our variational schemes are also stable on strongly deformed meshes while conserving mass and total energy to a high degree.

6.1 Internal gravity waves by hydrostatic adjustment

An essential ingredient of the derivation of Boussinesq, anelastic and pseudo-incompressible models is the assumption of a vertically varying reference state that is in hydrostatic balance, i.e. the gravitational and pressure terms compensate each other (cf. Section 2). When out of equilibrium, the system tends to a balanced state by the so-called hydrostatic adjustment process [10] by emitting internal gravity waves.

Here, we investigate the above derived variational integrators using the hydrostatic adjustment process. We study their dynamical behavior, long term energy and mass conservation properties, and their discrete dispersion relations. To this end, we initialize the Boussinesq scheme as in [4], and adapt the therein suggested test case to suit also for the anelastic and pseudo-incompressible schemes. This will allow us to compare quantitatively the simulation results of our schemes with each other and with those of [4].

We use for the simulations in this section a computation domain of dimension $(x, z) \in \mathcal{D} = [0, L_x] \times [0, L_z], L_x = 24\,\mathrm{m}, L_z = 1\,\mathrm{m}$, while imposing periodic boundary conditions in x-direction and free-slip boundary conditions at the upper and lower boundaries of the domain. We integrate for a time interval of 100 s (in correspondence to [4]) with a time step size of $\Delta t = 0.25\,\mathrm{s}$. Both regular and irregular computational meshes have a resolution of $2 \cdot 384 \times 20$ triangular cells (cf. Figure 6.1).

6.1.1 Hydrostatic adjustment of the Boussinesq model

Consider the Boussinesq system in hydrostatic equilibrium between a stable reference buoyancy $\bar{b}(z)$ and the pressure P_b of Section 2, i.e.,

$$\frac{\partial P_b}{\partial z} = \bar{b}. \tag{6.1}$$

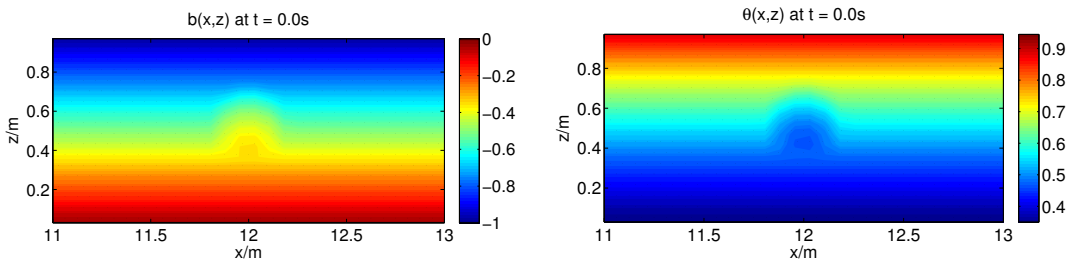

Figure 6.2: Initialization of the Boussinesq scheme by the buoyancy field $b(x, z, 0)$ shown left. Initalization of the anelasic and pseudo-incompressible schemes by the potential temperature field (cf. equations (6.8)) $\theta(x, z, 0)$ shown (right).

When out of equilibrium, the system tends to a hydrostatic balance by emitting internal gravity waves that obey the dispersion relation

$$\omega^2 = \frac{k_x^2 N_b^2}{\mathbf{k^2}} \tag{6.2}$$

with wave vector $\mathbf{k} = (k_x, k_y) \in \mathbb{Z}$ in which $N_b^2 := \frac{d\bar{b}}{dz} = \frac{g}{\theta_0}\frac{d\bar{\theta}}{dz}$, assumed to be a constant, denotes the Brunt-Väsälä frequency for the case of Boussinesq equations. One observes that the frequencies of the internal gravity waves are bounded from above by N_b.

We further note that mass conservation is given by

$$\frac{d}{dt}\int_{\mathcal{D}} b(x, z, t) d\mathbf{x} = 0. \tag{6.3}$$

Being implicitly related to the density, we refer to this quantity, and the upcoming similar ones for anelastic and pseudo-incompressible equations, generally as mass $M(t)$. Hence, we study whether the discrete integral of b over the domain $\mathcal{D}$, denoted as mass $M(t)$, remains constant in time and whether the discrete total energy, analogously to (2.5), is conserved.

Initialization. Analogously to [4], we initialize the system on the basis of a hydrostatic equilibrium, given by $u_{\text{eq}}(x, z) = w_{\text{eq}}(x, z) = 0$ and $b_{\text{eq}}(x, z) = -N_b^2 z =: \bar{b}(z)$, on which at $t = 0$ a localized positive buoyancy disturbance $\tilde{b}(x, z)$ with compact support is superimposed. Hence, the initial buoyancy field $b(x, z, 0) = \bar{b}(z) + \tilde{b}(x, z)$ with Brunt-Väsälä frequency $N_b = 1/\text{s}$ is given by the function

$$b(x, z, 0) = N_b^2 \begin{cases} -z + \beta_b e^{\left(\frac{-r_0^2}{r_0^2 - r^2}\right)} & \text{if } r < r_0, \quad r^2 = (x - \frac{L_x}{2})^2 + (z - \frac{L_z}{2})^2, \\ -z & \text{if } r \geq r_0, \end{cases} \tag{6.4}$$

with parameters: $r_0 = 0.2 \cdot L_z$, $\beta_b = 0.3 \cdot L_z$, $r^2 = (x - \frac{L_x}{2})^2 + (z - \frac{L_z}{2})^2$. Note that $[z] = \text{m}$, hence the choice of $N_b = 1/\text{s}$ suggests further to set $g = 1\,\text{m/s}^2$ and $\theta_0 = 1\,\text{K}$. Given these analytical functions, the discrete function $B = \{B_i | \text{ for all triangles } T_i\}$ is obtained by setting $B_i(0) = b(x_i, z_i, 0)$ for all triangles T_i with cell centers at position (x_i, z_i).

Results. To study numerically the dispersion relation of our discrete model, we determine the Fourier transforms of a time series of the buoyancy field $b(x, z, t)$ for the time interval

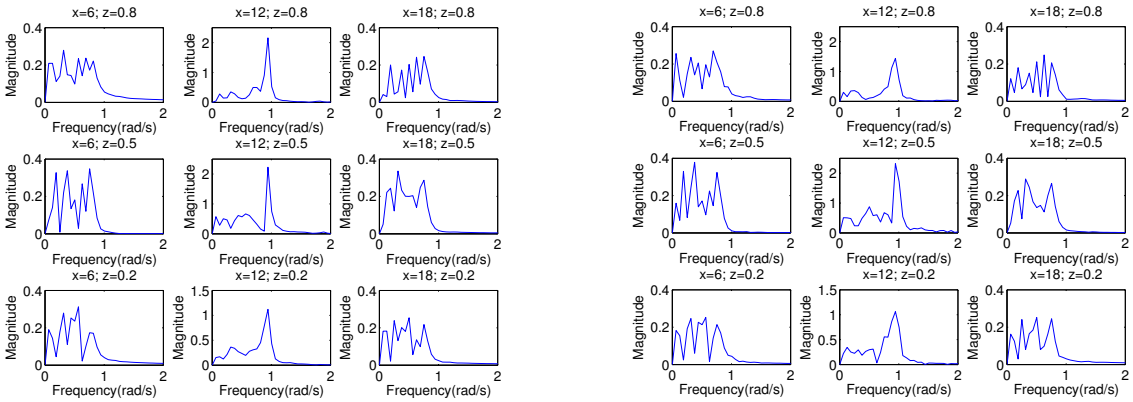

Figure 6.3: Boussinesq scheme: frequency spectra for regular (left block) and irregular (right block) meshes determined on various points in the domain $\mathcal{D}$. The position in the panel indicates the corresponding position in $\mathcal{D}$, for instance the upper left panel corresponds to a point at the upper left of $\mathcal{D}$.

$t \in [0, 100\,\mathrm{s}]$ at various locations of the computation domain $\mathcal{D}$ (similar to those chosen by [4]). The resulting spectra are presented in Figure 6.3. For all selected sample points, these spectra show an anisotropy manifested by the fact that they are bound from above by $N_b = 1/\mathrm{s}$. For the central point, the spectrum is pronounced for values of N_b, in well agreement with equations (6.2): for waves with frequency near N_b, the group velocity tends to zero leaving the corresponding waves trapped in the center of the domain. A very similar distribution of frequency spectra within the domain $\mathcal{D}$ has been found by [4]. The simulations on irregular meshes give very similar frequency spectra.

Figure 6.4 shows for regular (left column) and irregular (right column) meshes snapshots of the buoyancy field $b(x, z, t)$ at times $t = 5\,\mathrm{s}$ and $t = 8\,\mathrm{s}$ for a region $[11\,\mathrm{m}, 13\,\mathrm{m}] \times [0, 1\,\mathrm{m}]$. For these early times, before waves that are reflected by the boundaries reach the center, one clearly observes the internal gravity waves, caused by the buoyancy perturbation, that propagate from the center along the channel in x-direction. Besides of small irregularities of the solutions on irregular meshes, in particular visible at the velocity field that is not completely symmetric with respect to the axis $x = 10\,\mathrm{m}$, the results obtained either on regular or irregular meshes are very similar.

Figure 6.5 illustrates for regular (left column) and irregular (right column) meshes the time evolution of the relative errors (determined as ratio of current values at t over initial value at $t = 0$) of total energy $E_{tot}(t)$ (upper panels) and mass $M(t)$ of equations (6.3) (lower panels). The middle panels show the energy transfer between kinetic $E_k(t)$ and potential $E_p(t)$ energy such that the sum of both energy sources, $E_{tot}(t)$, is conserved. One realizes that the initial surplus of potential energy, caused by the superimposed disturbance on the equilibrium state, triggers an oscillatory transfer between both energy sources.

As one can further deduce from these plots, the total energy shows an oscillatory behavior while being very well conserved in the mean for long integration times. Being symplectic, our variational integrator hence fulfills the expected behavior. The magnitude of oscillation is in the order of 10^{-6}, but depends on the time step size; here we used $\Delta t = 0.25\,\mathrm{s}$. Reducing the time step size by a factor of 10 decreases simultaneously the magnitude of the relative errors in

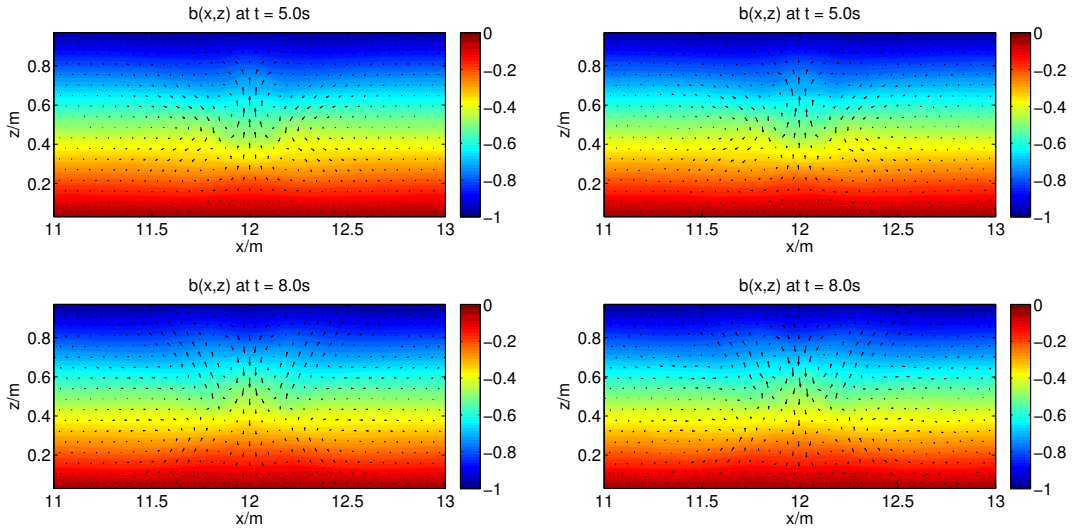

Figure 6.4: Boussinesq scheme: snapshots of the wave propagation on regular (left column) and irregular (right column) meshes.

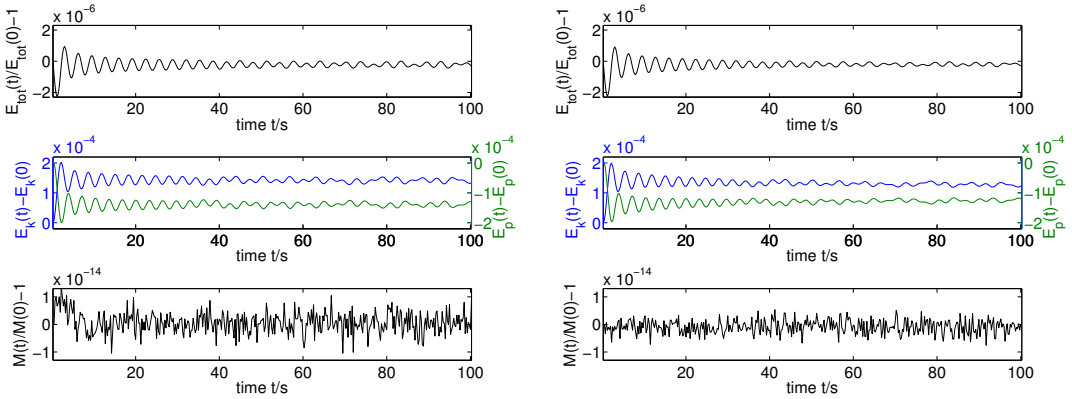

Figure 6.5: Boussinesq scheme: relative errors of total energy $E_{tot}(t)$ and mass $M(t)$, and energy transfer between kinetic $E_k(t)$ and potential $E_p(t)$ energy, for regular (left block) and irregular (right block) meshes.

total, kinetic, and potential energy by the same factor (not shown). Hence, our scheme shows the expected 1st-order convergence rate with time (cf. time scheme derivation in [14]). The mass $M(t)$ is conserved with an order of 10^{-15}. The quantities of interest for the simulations on irregular meshes are equally well conserved as on regular meshes.

6.1.2 Hydrostatic adjustment of the anelastic model

We consider the anelastic equations in hydrostatic equilibrium. By assuming that the reference states $\bar{\rho}(z)$ and $\bar{\theta}(z)$ are such that

$$N^2 = \frac{g}{\bar{\theta}}\frac{d\bar{\theta}}{dz} \quad \text{and} \quad \sigma_{\mathrm{a}} = \frac{1}{4}\left(\frac{1}{\bar{\rho}}\frac{d\bar{\rho}}{dz}\right)^2 - \frac{1}{2}\frac{d}{dz}\left(\frac{1}{\bar{\rho}}\frac{d\bar{\rho}}{dz}\right) \tag{6.5}$$

are constant numbers, the dispersion relation takes the simple form

$$\omega^2 = \frac{N^2 k_x^2}{\mathbf{k}^2 + \sigma_a}. \tag{6.6}$$

Constant values for N and σ_a are obtained by taking $\bar{\theta}(z) = \alpha e^{\frac{N^2}{g} z}$ and $\bar{\rho}(z) = \beta e^{Kz}$, in which case $\sigma_a = \frac{K^2}{4}$.

Analogously to equations (6.2), also this dispersion relation shows an anisotropic spectra that is bound from above by N. To see this, consider the extremes of (6.6): the lower bound at $\min(\omega) = 0$ results from $k_x = 0$ while the upper bound $\max(\omega) = N$ results for $k_x \gg k_y, \sigma$.

For the anelastic equations, mass conservation is given by

$$\frac{d}{dt} \int_{\mathcal{D}} \bar{\rho}(z)\theta(x, z, t) d\mathbf{x} = 0, \tag{6.7}$$

as $\int_{\mathcal{D}} \bar{\rho}\partial_t \theta d\mathbf{x} = -\int_{\mathcal{D}} \mathbf{d}\theta \cdot \bar{\rho}\mathbf{u} d\mathbf{x} = -\int_{\mathcal{D}} \operatorname{div}(\bar{\rho}\mathbf{u}\theta) d\mathbf{x} + \int_{\mathcal{D}} \operatorname{div}(\bar{\rho}\mathbf{u})\theta d\mathbf{x} = 0$, which follows by the anelastic constraint $\operatorname{div}(\bar{\rho}\mathbf{u}) = 0$ and by the choice of boundary conditions, i.e. $\mathbf{u} \cdot \mathbf{n} = 0$, on $\partial\mathcal{D}$. We study if our anelastic discretization scheme conserves the latter quantity and if the total discrete energy, a discrete version of $E = \bar{\rho}\left(\frac{1}{2}|\mathbf{u}|^2 + c_p \bar{\pi}\theta\right)$ is well conserved, too.

Initialization. We aim for an initialization that produces results comparable to the Boussinesq scheme and that meets the requirements of constant N and σ_a in equations (6.5). To this end, the hydrostatic equilibrium is set up by $u_{\text{eq}}(x, z) = w_{\text{eq}}(x, z) = 0$ and a reference state $\bar{\theta}(z) = e^{z+c}$ for a constant c, on which at $t = 0$ a negative potential temperature perturbation $\tilde{\theta}(x, z)$ is superimposed. The initial potential temperature field $\theta(x, z, 0) = \bar{\theta}(z) + \tilde{\theta}(x, z)$ is hence given by

$$\theta(x, z, 0) = \begin{cases} e^{z+c} - \beta_a e^{\left(\frac{-r_0^2}{r_0^2 - r^2}\right)} & \text{if } r < r_0, \quad r^2 = (x - \frac{L_x}{2})^2 + (z - \frac{L_z}{2})^2, \\ e^{z+c} & \text{if } r \geq r_0, \end{cases} \tag{6.8}$$

with parameters $r_0 = 0.2 \cdot L_z$ and $\beta_a = 0.2 \cdot L_z$.

To obtain a potential temperature field with comparable magnitude (in the order of $\theta_0 = 1\,\text{K}$) to the buoyancy field – but now with increasing value with height z as it would be in the atmosphere – we set $c = -L_z = -1$ (corresponding to $\alpha = 1/e$ from above) giving 0.4 K at the bottom and 1 K at the top of the domain. Note that β_a is slightly smaller than β_b of equations (6.4); it is chosen such that at the domain center x_c, z_c, there is $\theta(x_c, z_c, 0) \approx -b(x_c, z_c, 0)$ which results in similar magnitudes of oscillation. With this choice of θ, the Brunt-Väisälä frequency is $N^2 = \frac{g}{\bar{\theta}} \frac{d\bar{\theta}}{dz} = 1/\text{s}^2$, where we set $g = 1\,\text{m/s}^2$. This setup will allow us to compare the results obtained by the anelastic with those of the Boussinesq scheme from above and with those in [4].

The requirement that σ_a is constant, restricts our choice of the stratified density field $\bar{\rho}$ to be either a constant or an exponential function. We study our scheme using two profiles: (i) $\bar{\rho}(z) = e^{-z}$, which is very similar to a realistic stratification, and (ii) $\bar{\rho}(z) = e^{-8z}$ providing a very strongly stratified density field. To remain concise, we only present the frequency spectra for both profiles, while we restrict our representation elsewhere to the realistic profile and only comment on results obtained when using the strong density stratification.

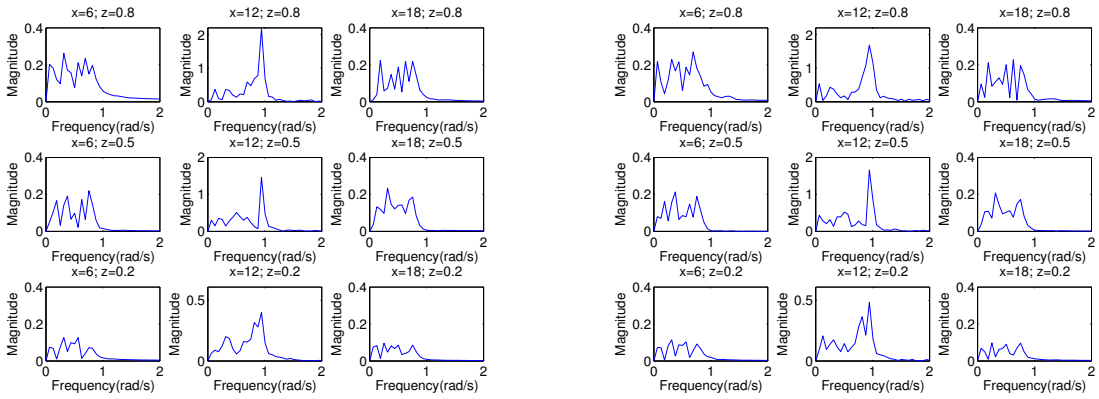

Figure 6.6: Anelastic scheme: frequency spectra for initialization (i) with $\bar{\rho}(z) = e^{-z}$ for regular (left block) and irregular (right block) meshes determined on various points in the domain $\mathcal{D}$ similarly to Fig. 6.3.

The relation between $\bar{\pi}$ and $\bar{\theta}$, see (2.2), allows us to initialize the Exner pressure by the potential temperature field via

$$\bar{\pi}(z) = \frac{g}{c_p} e^{-(z+c)} \,. \tag{6.9}$$

for any values of specific heat at constant pressure c_p (here we set $c_p = 1$), as it will cancel out in the anelastic equations.

Given these functions, the discrete ones are obtained by setting $\Theta_i(0) = \theta(x_i, z_i, 0)$, $\bar{\Pi}_i = \bar{\pi}(x_i, z_i)$ and $\bar{\rho}_i = \bar{\rho}(x_i, z_i)$ for all triangles T_i with cell centers at position (x_i, z_i).

Results. Similarly to the Boussinesq scheme, we determine the frequency spectra by taking Fourier transforms of a time series of the potential temperature field $\theta(x, z, t)$ for the time interval $t = [0, 100\,\mathrm{s}]$ at locations in $\mathcal{D}$ similar to those in Section 6.1.1. Figure 6.6 shows the various frequency spectra for initialization (i) $\bar{\rho}(z) = e^{-z}$; left block for the regular, and right block for the irregular meshes. These spectra consist of frequencies lying between zero and $\max(\omega) = N = 1/\mathrm{s}$, which agrees well with the frequency pattern in Figure 6.3 and reflects very well the properties of the analytical dispersion relation (6.6).

Using strong stratification (density initialization (ii) $\bar{\rho}(z) = e^{-8z}$), the spectra shown in Figure 6.7 for both mesh types are similar to Figure 6.6, in particular their lower and upper boundaries. The distribution of occupied wave numbers though slightly differs from initialization (i): the upper panels show in general higher magnitude, the central panels show increased magnitude of small wave numbers, while the peaks at $N = 1/\mathrm{s}$ are not as distinct as for the weaker density stratification. In case of strong stratification, the magnitudes of oscillation are strongest at the upper boundary, i.e. in the region with lowest density. This causes small scale waves (noise) that are distributed over the domain and that occupy the small waves numbers in the spectra.

In Figure 6.8, we show snapshots of the potential temperature $\theta(x, z, t)$ at time $t = 5\,\mathrm{s}$ and $t = 8\,\mathrm{s}$ for the region $[11\,\mathrm{m}, 13\,\mathrm{m}] \times [0, 1\,\mathrm{m}]$ using the realistic density profile (i). Comparing with Figure 6.4, the velocity and potential temperature fields for both time instances and both mesh types are rather similar to those obtained with the Boussinesq scheme, noticing that the magnitude of displacement of θ from equilibrium is more enhanced in the anelastic case. Again,

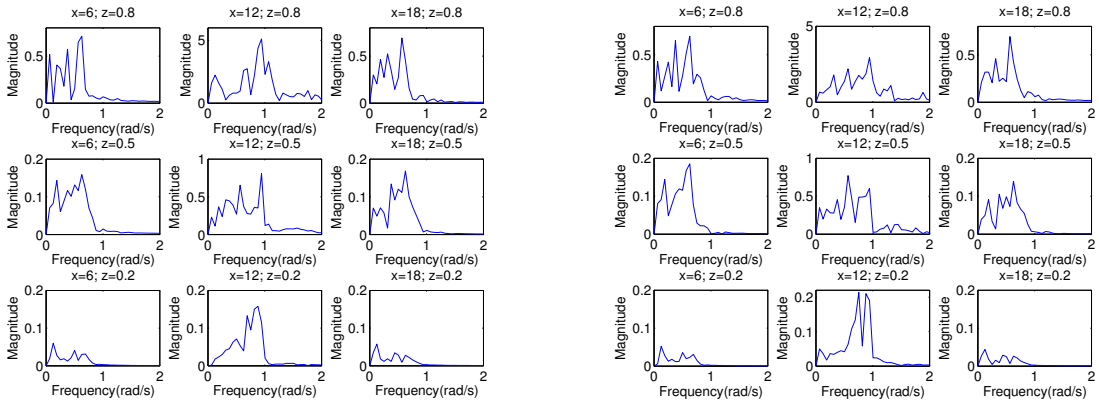

Figure 6.7: Anelastic scheme: frequency spectra for initialization (i) with $\bar{\rho}(z) = e^{-8z}$ for regular (left block) and irregular (right block) meshes determined on various points in the domain $\mathcal{D}$ similarly to Figure 6.3. The spectra of the pseudo-incompressible scheme using this initialization show very similar pattern (not shown).

the irregular meshes (right column) trigger solutions that are slightly non axis-symmetric with respect to $x = 10\,\mathrm{m}$, but agree in general very well with the internal gravity wave propagations obtained on regular meshes.

Figure 6.9 shows the relative errors of total energy (upper panels) and mass of equations (6.7) (lower panels) for regular (left column) and irregular (right column) meshes. Again, the central panels show the energy transfer between kinetic and potential energy. In all cases, these quantities are as well conserved as for the Boussinesq scheme, in particular their mean is very well conserved for long integration times. The conservation of mass shows a slight growth (in particular for the irregular mesh), but within the order of 10^{-13} on a very acceptable level. For these plots we used a time step size of $\Delta t = 0.25\,\mathrm{s}$. Similar to above, the anelastic scheme shows the expected 1st-order convergence rate with time (cf. Section 6.1.1 for more details).

Remark 6.1 By setting $\bar{\rho} = \rho_0$ and $\bar{\theta} = \theta_0$ as constants, the analytical Boussinesq and anelastic models agree. By initializing the discrete schemes in equations (5.5) and (5.9) accordingly, i.e. by setting $\theta = -b$, $\bar{\rho} = 1$, $\bar{\theta} = \theta_0 = 1$, and $c_p = 1$, we could exactly recover the numerical results of the Boussinesq by the anelastic scheme (not shown).

6.1.3 Hydrostatic adjustment of the pseudo-incompressible model

We consider the pseudo-incompressible equations in hydrostatic equilibrium. By assuming that the reference states $\bar{\rho}(z)$ and $\bar{\theta}(z)$ are such that

$$N^2 = \frac{g}{\bar{\theta}}\frac{d\bar{\theta}}{dz} \quad \text{and} \quad \sigma_{\mathrm{pi}} = \left(\frac{1}{\bar{\theta}}\frac{d\bar{\theta}}{dz} + \frac{1}{2\bar{\rho}}\frac{d\bar{\rho}}{dz}\right)^2 - \frac{d}{dz}\left(\frac{1}{\bar{\theta}}\frac{d\bar{\theta}}{dz} + \frac{1}{2\bar{\rho}}\frac{d\bar{\rho}}{dz}\right) \tag{6.10}$$

are constant numbers, the dispersion relation takes the simple form

$$\omega^2 = \frac{N^2 k_x^2}{\mathbf{k}^2 + \sigma_{\mathrm{pi}}}. \tag{6.11}$$

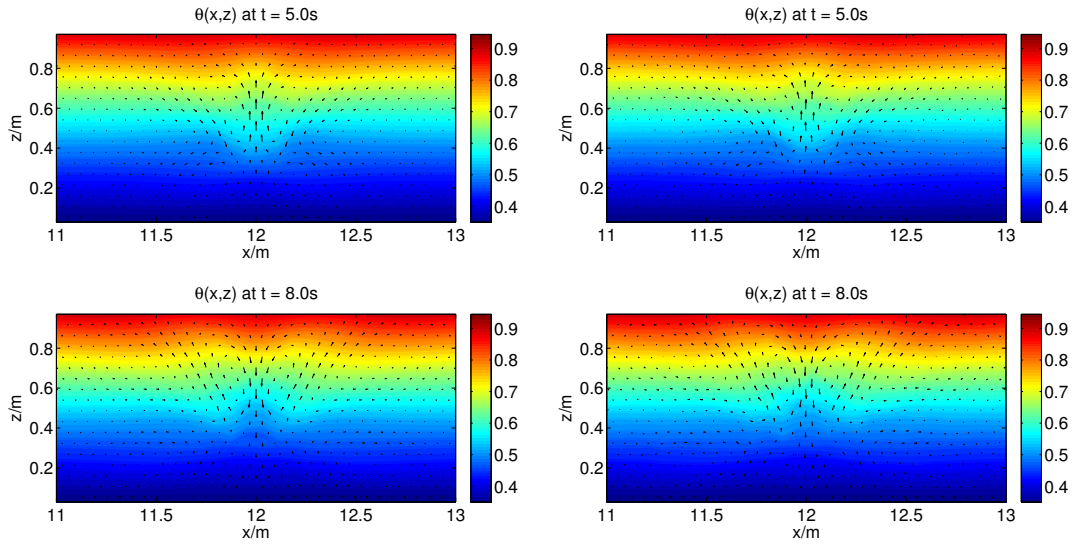

Figure 6.8: Anelastic scheme: snapshots of the wave propagation on regular (left column) and irregular (right column) meshes for $\bar{\rho}(z) = e^{-z}$

Therefore, the dispersion relation (6.11) is anisotropic and bound from above by $\max(\omega) = N$ just as for the Boussinesq and anelastic models, which results from the same reasoning as done for equation (6.6).

For the pseudo-incompressible equations, we note that the mass conservation is given by

$$\frac{d}{dt}\int_{\mathcal{D}} \bar{\rho}(z)\bar{\theta}(z)\theta(x,z,t)d\mathbf{x} = 0, \tag{6.12}$$

which follows by a similar argumentation as presented for equation (6.7).

Initialization. The pseudo-incompressible scheme is initialized exactly as the anelastic scheme with the only difference that here we do not need to define the Exner pressure $\bar{\pi}(z)$ (cf. equation (5.13)). In particular, by choosing exponential functions for the potential temperature and the density fields, that is $\bar{\theta}(z) = e^{z}$ and (i) $\bar{\rho}(z) = e^{-z}$ or (ii) $\bar{\rho}(z) = e^{-8z}$, we guarantee that the conditions put on N and σ_{pi} to be constant, required to be able to calculate the dispersion relation (6.11), are fulfilled. As above, we study the dynamics, the conservation of the quantities of interest, and the dispersion relations for the two different density stratifications (i) and (ii).

Results. Analogously to Section 6.1.2, we determine the frequency spectra by taking Fourier transforms of a time series of $\theta(x,z,t)$ for the time interval $t = [0, 100\,\text{s}]$ at various locations in $\mathcal{D}$. Figure 6.10 shows the resulting frequency spectra for initialization (i) $\bar{\rho}(z) = e^{-z}$; left block for the regular, and right block for the irregular mesh. These spectra show for both regular and irregular meshes a very similar pattern as in Figure 6.6, in particular the maximal frequencies at each panel drop strongly at $\max(\omega) = 1/\text{s}$ as theoretically expected. When using initialization (ii), the spectra for both regular and irregular meshes are similar to those presented in Figure 6.7 for the anelastic case; one observes also here an increase of small wave numbers occupying the frequency spectra, in particular on the upper panels (not shown).

In Figure 6.11, we show snapshots of the potential temperature $\theta(x,z,t)$ at time $t = 5\,\text{s}$ and $t = 8\,\text{s}$ for a region $[11\,\text{m}, 13\,\text{m}] \times [0, 1\,\text{m}]$ and for the density profile (i). They show for

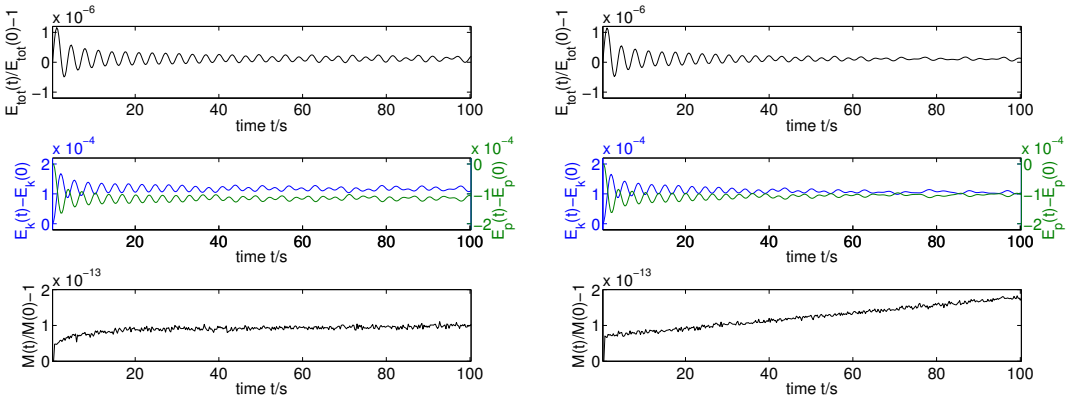

Figure 6.9: Anelastic scheme: relative errors of total energy $E_{tot}(t)$ and mass $M(t)$, and energy transfer between kinetic $E_k(t)$ and potential $E_p(t)$ energy, for regular (left block) and irregular (right block) meshes.

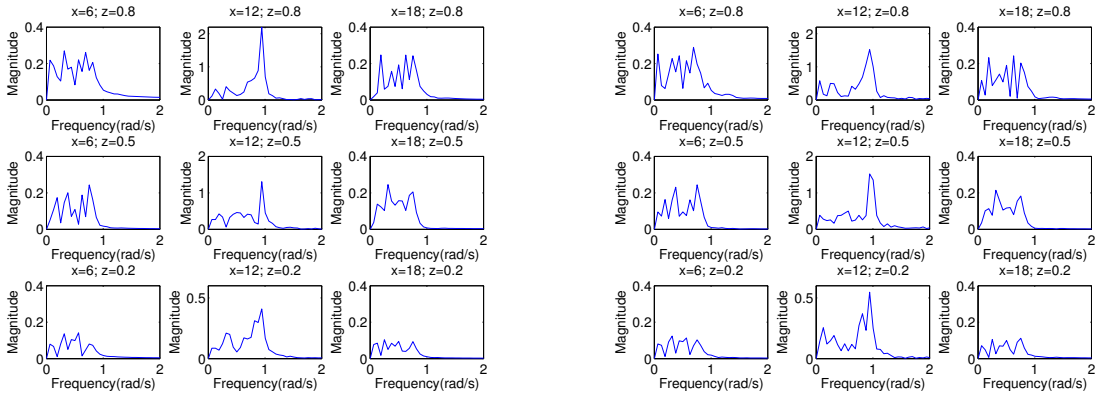

Figure 6.10: Pseudo-incompressible scheme: frequency spectra for initialization (i) with $\bar{\rho}(z) = e^{-z}$ for regular (left block) and irregular (right block) meshes determined on various points in the domain $\mathcal{D}$ similarly to Figure 6.3.

both time instances and both mesh types very similar dynamical behavior as for Boussinesq and anelastic cases.

Figure 6.12 shows the relative errors of total energy and mass of equation (6.12) and the energy transfer between kinetic and potential energy. On both mesh types, the errors are in the same order as for the Boussinesq and anelastic schemes. Also here, the time step size is $\Delta t = 0.25\,\mathrm{s}$ and the scheme shows the expected 1st-order convergence rate with time. The time evolution of mass shows a slight decline, but only in the order of 10^{-14}, hence it is very well conserved.

6.2 Rising and falling bubble test cases

On advection dominated test cases, namely (i) a rising hot bubble in a cold environment and (ii) a cold drop of air in a warm environment, we illustrate the dynamics of the anelastic and pseudo-incompressible schemes. We point out the similarities and differences between the underlying approximations and we test whether our variational integrators share these properties.

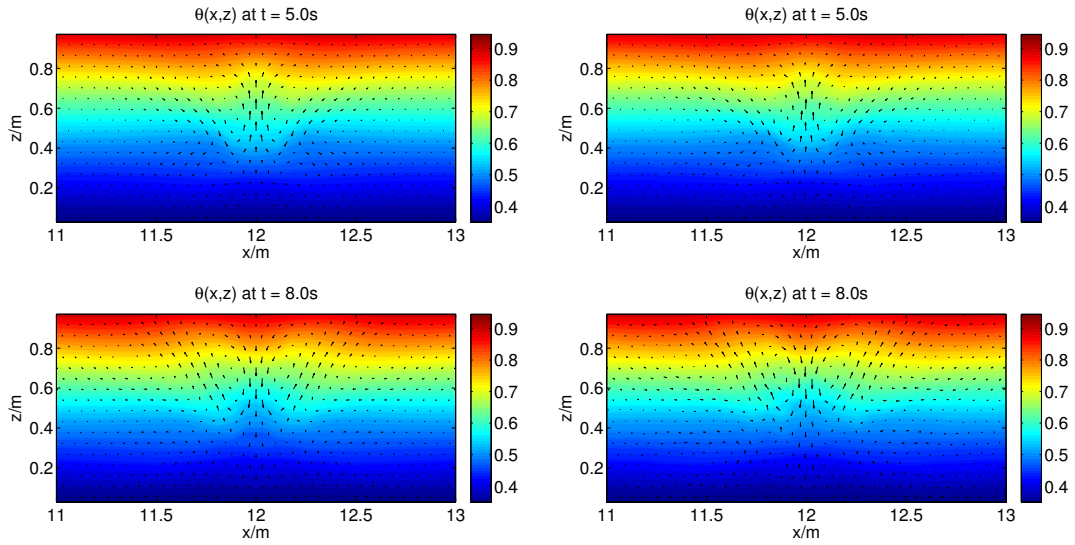

Figure 6.11: Pseudo-incompressible scheme: snapshots of the wave propagation on regular (left column) and irregular (right column) meshes for $\bar{\rho}(z) = e^{-z}$.

6.2.1 Rising bubble test cases

Using the test case of a rising hot bubble of air in a cold environment, we will verify in the following that in case of small potential temperature variations, the anelastic and pseudo-incompressible schemes behave very similarly. In order to enable quantitative comparisons also with literature, we set up the test case similarly to [9].

Initialization. We use a domain of dimension $(x, z) \in [0, L_x] \times [0, L_z], L_x = 20\,\text{km}, L_z = 10\,\text{km}$, with periodic boundary condition in x-direction and free-slip boundary conditions at the upper and lower boundaries of the domain. The regular and irregular meshes have a resolution of $2 \cdot 321 \times 186$ cells and we use a time step size of $\Delta t = 2.5\,\text{s}$.

The potential temperature distribution consisting of a constant background state $\bar{\theta} = 300\,\text{K}$ and some initial disturbance $\theta'(x, z, 0)$ is given by

$$\theta(x,z,0) = 300\,\text{K} + \begin{cases} \delta\theta \cos^2\left(\frac{\pi}{2} r\right) & \text{for } r \le 1,\ r = 5\sqrt{\left(\frac{x-\frac{1}{2}L_x}{L}\right)^2 + \left(\frac{z-\frac{1}{2}L_z}{L} + z_{\text{off}}\right)^2}, \\ 0 & \text{otherwise,} \end{cases} \tag{6.13}$$

with values for $\delta\theta = 2\,\text{K}$, $L = 10\,\text{km}$, and $z_{\text{off}} = 0.03\,L$. This results in an Exner pressure $\bar{\pi}(z) = -\frac{g}{c_p \bar{\theta}} z$ with $\bar{\pi}(z = 0) = 0$ according to (2.2).

The hydrostatic background density stratification shall be described by (cf. [13])

$$\bar{\rho}(\hat{z}) = \frac{P_{ref}}{R\bar{\theta}} \left(1 - \beta\hat{z}\right)^{\frac{1}{\gamma-1}}, \qquad \beta = \frac{gL_z}{c_p\bar{\theta}}, \qquad \hat{z} = \frac{z}{L_z}, \tag{6.14}$$

$$\bar{\rho}(z) = \left(1 - 0.3\frac{z}{L_z}\right)^{\frac{5}{2}}, \quad \text{for } z \in [0, L_z]. \tag{6.15}$$

For the parameters, we have chosen typical values for a dry atmosphere: isentropic exponent $\gamma = 1.4$, specific heat of $c_p = 1000\,\frac{\text{J}}{\text{K kg}}$, gas constant of $R = 287\,\frac{\text{J}}{\text{K kg}}$, a reference pressure of

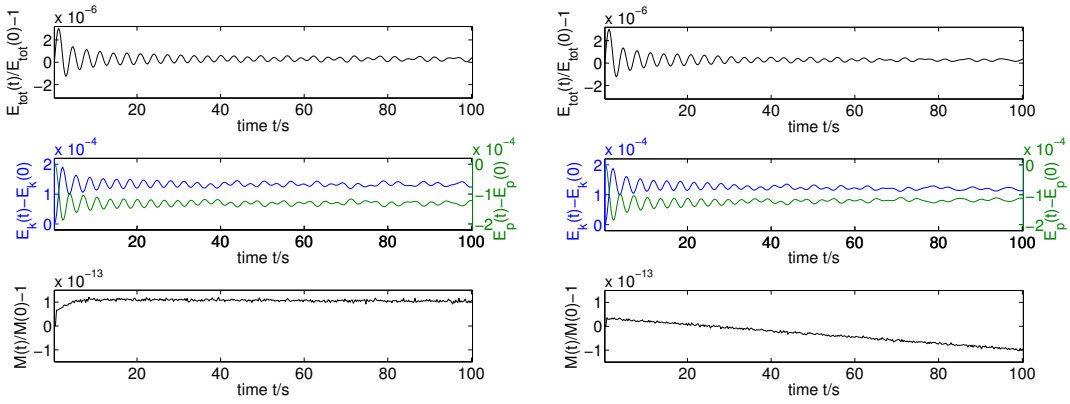

Figure 6.12: Pseudo-incompressible scheme: relative errors of total energy $E_{tot}(t)$ and mass $M(t)$, and energy transfer between kinetic $E_k(t)$ and potential $E_p(t)$ energy, for regular (left block) and irregular (right block) meshes.

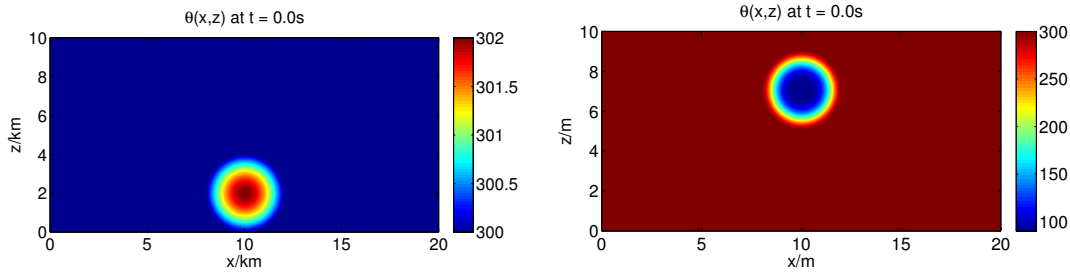

Figure 6.13: Initial conditions: on the left for the warm bubble test case, on the right for the cold bubble test case with $\delta\theta = 210\,\mathrm{K}$ (cf. Section 6.2.2).

$P_{ref} = 10^5\,\frac{\mathrm{kg}}{\mathrm{m\,s^2}}$ and a gravitational acceleration of $g = 10\,\frac{\mathrm{m}}{\mathrm{s^2}}$; leading to $\beta \approx 0.3$ and $\frac{P_{ref}}{R\bar{\theta}} \approx 1$. For $z = 0$, equation (6.15) gives $\bar{\rho}(z = 0) = 1\,\frac{\mathrm{kg}}{\mathrm{m\,s^2}}$ (in agreement with [9]). Using this analytical functions we initialize the discrete ones as described above.

Using this initialization, we expect to obtain results very similar to those of Klein [9]. As the integration time with 1000 s is such that the bubble does not interact with the boundaries and as the initialization is axis-symmetric to $x_c = 10\,\mathrm{km}$ (cf. Figure 6.13), the difference in the choice of boundary conditions for our setup and that in [9] does not influence the results.

Results. Figure 6.14 shows the potential temperature $\theta(x, z, t)$ for the anelastic (left column) and pseudo-incompressible schemes (right column) for regular (upper row) and irregular (lower row) meshes after an integration of 1000 s. The initial data are symmetric with respect to vertical axis $x_c = 10\,\mathrm{km}$. As the initial maximum of potential temperature is located on this symmetry line and as the boundary conditions are mirror-symmetric too, the maximum value should stay on the symmetric line and it's value should be conserved during the integration.

Choosing the initialization of Klein [9], we are able to directly compare the results. First we note that the results for the anelastic and pseudo-incompressible schemes under small variations in potential temperature (i.e. $\theta_{max}/\theta_{min} = 302\,\mathrm{K}/300\,\mathrm{K}$) are almost indistinguishable, in agreement with [9]. This is true for both regular and irregular meshes. Moreover, both schemes present well the advection speed of the bubbles reaching a height of 8 km after an integration

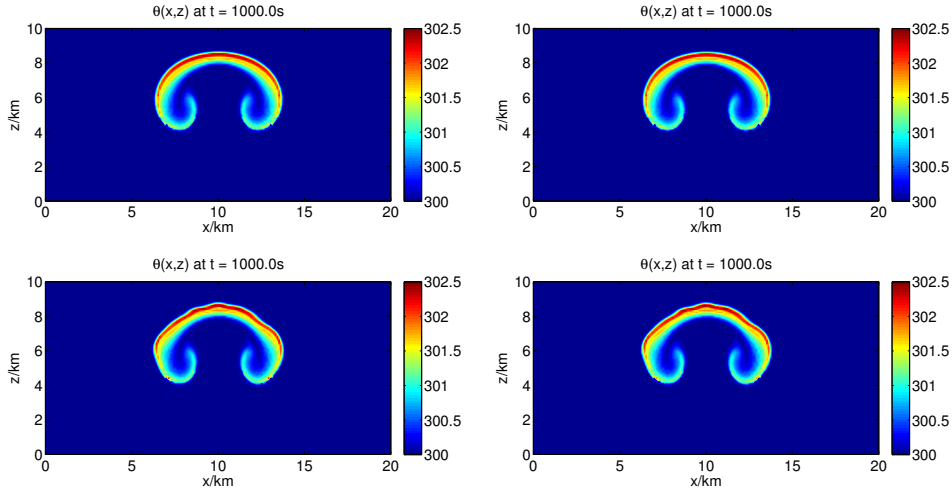

Figure 6.14: Potential temperature at $t = 1000\,\mathrm{s}$ for the anelastic (left column) and pseudo-incompressible schemes (right column) on regular (upper row) and irregular (lower row) meshes.

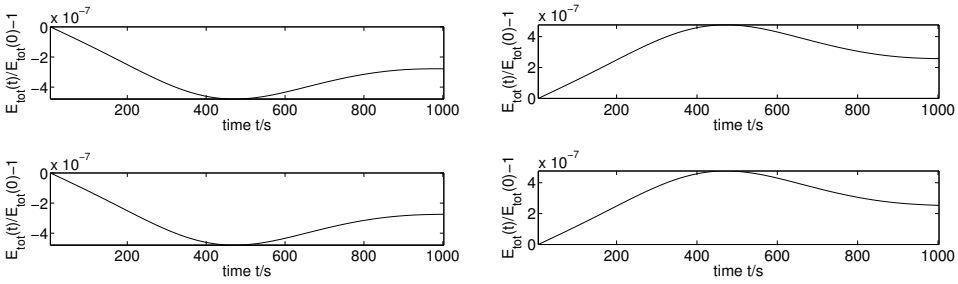

Figure 6.15: Relative error in total energy for the anelastic (left column) and pseudo-incompressible schemes (right column) for regular (upper row) and irregular meshes (lower row) for the warm bubble test case.

of 1000 s, in well agreement with literature.

As to the symmetry of the solutions, anelastic and pseudo-incompressible schemes on regular meshes show nicely the required symmetry behavior while the maxima stay indeed on the symmetry line, but increases to $\theta_{\max} = 2.5\,\mathrm{K}$. This is in contrast to [9], in which the solution develops two local extrema located symmetrically some finite distance away from the symmetry line while the maximal value of θ reaches, in their best case simulations, $\theta_{\max} = 1.73K$. These latter results had been obtained by using a scheme that applies flux limiters that avoid the development of too steep gradients of θ. As our schemes do not apply such flux limiters, or any kind of smoothing methods, such steep gradients develop, in particular for latter times when the bubble is strongly stretched, leading to the increased maximal potential temperature values.

Using irregular meshes for the variational anelasic and pseudo-incompressible schemes, the general dynamical behavior of the rising bubble and, in particular, the symmetry of the solutions are well represented. Only the shapes of the stretched bubbles show some wiggles that result from the distorted triangles on the irregular meshes. Here, the maximal values of potential temperature is about $\theta_{\max} = 2.8\,\mathrm{K}$.

From Figure 6.15 we deduce that for regular and irregular meshes both anelasic and pseudo-

incompressible schemes conserve very well the total energy in the order of 10^{-6} and that, for each scheme, there is almost no difference of the results obtained on either regular or irregular meshes. For all cases, the mass as defined in equations (6.7) and (6.12) is conserved in the order of 10^{-14} (not shown).

6.2.2 Cold bubble test case

Finally we study the different behavior of the variational anelastic and pseudo-incompressible schemes in case of large potential temperature variations. Again, we set up the test case similarly to [9] which allow us to compare the results.

Initialization. The computational domain is given by $(x, z) \in [0, L_x] \times [0, L_z]$, $L_x = 20\,\mathrm{m}$, $L_z = 10\,\mathrm{m}$, with periodic boundary condition in x-direction and free-slip boundary conditions in z-direction. Also here, we calculate on regular and irregular meshes with a resolution of $2 \cdot 321 \times 186$ triangles. We use a time step size of $\Delta t = 0.0125\,\mathrm{s}$.

The potential temperature distribution consisting of a constant background state $\bar{\theta} = 300\,\mathrm{K}$ and some initial disturbance $\theta'(x, z, 0)$ is given by

$$\theta(x, z, 0) = 300\,\mathrm{K} - \begin{cases} \frac{\delta\theta}{2}(1+\cos(\pi r^2)) & \text{for } r \leq 1,\ r = 5\sqrt{\left(\frac{x-\frac{1}{2}L_x}{L}\right)^2 + \left(\frac{z-\frac{1}{2}L_z}{L} + z_{\text{off}}\right)^2}, \\ 0 & \text{otherwise,} \end{cases} \tag{6.16}$$

with values for $\delta\theta = 30\,\mathrm{K}$ and $210\,\mathrm{K}$, $L = 10\,\mathrm{m}$, and $z_{\text{off}} = -0.02\,L$. The Exner pressure $\bar{\pi}(z)$ required for the anelastic, and the background density stratification $\bar{\rho}(z)$ required for both schemes are the same as in the warm bubble test case. Using this analytical functions we initialize the discrete ones as described above.

Analogously to the warm bubble case, by using this initialization we expect to obtain very similar results to those presented in Klein [9], as also for this test case the bubble does not interact with the boundaries and as the initialization is axis-symmetric to $x_c = 10\,\mathrm{m}$ (cf. Figure 6.13).

Results. Figure 6.16 shows the potential temperature fields of the falling cold air bubble with $\delta\theta = 30\,\mathrm{K}$ (upper row) and $\delta\theta = 210\,\mathrm{K}$ (lower row) for the anelastic (left column) and pseudo-incompressible schemes (right column) on regular meshes. We realize that for small potential density variations, the anelastic and pseudo-incompressible schemes give very similar results (upper row), as already verified above for the warm bubble test case. For larger density variations though, the corresponding potential temperature fields obviously differ (cf. lower row). The results obtained on irregular meshes are almost indistinguishable from those presented in Figure 6.16 (hence not shown).

The differences between the anelastic and pseudo-incompressible models are caused by the different pressure gradient terms, i.e by the, in time, linear term $\nabla(\bar{\theta}\pi)$ for the anelastic and by the nonlinear term $\theta\nabla\pi$ for the pseudo-incompressible models, as explained in the following. The shape of the bubble in the anelastic case (left column of Figure 6.16) is mainly cause by the horizontal variation of buoyancy force, with maximum value at the symmetry axis $x_c = 10\,\mathrm{m}$. There, the air is the heaviest and will fall the fastest, with decreasing values to either the right or left hand side. This gradient in fall velocity will cause negative vorticity on the right and positive vorticity on the left of x_c, stretching the initial round bubble into a thin sheet. This, so

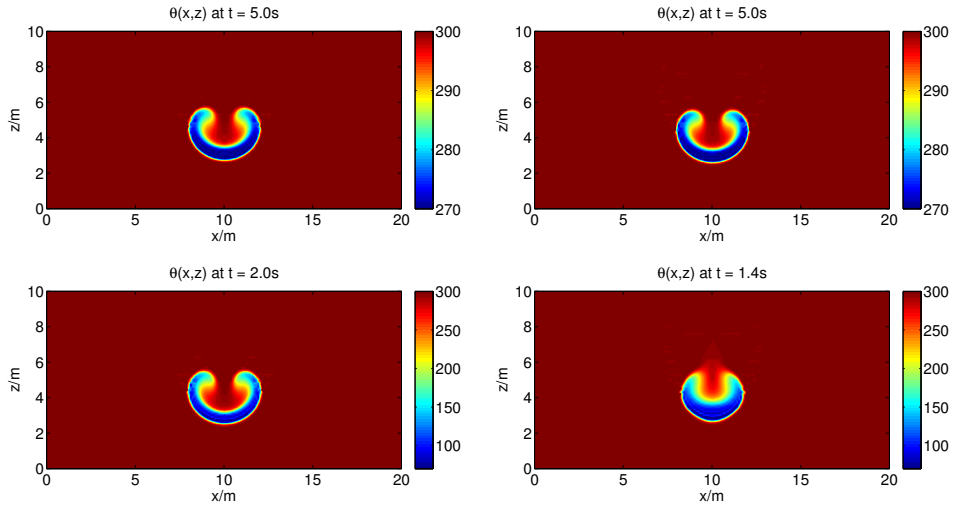

Figure 6.16: Potential temperature on regular meshes: comparison of results of the anelastic (left column) and pseudo-incompressible schemes (right column) for the falling cold air bubble; upper row: $\theta_{min}/\theta_{max} = 270\,\mathrm{K}/300\,\mathrm{K}$, lower row: $\theta_{min}/\theta_{max} = 90\,\mathrm{K}/300\,\mathrm{K}$.

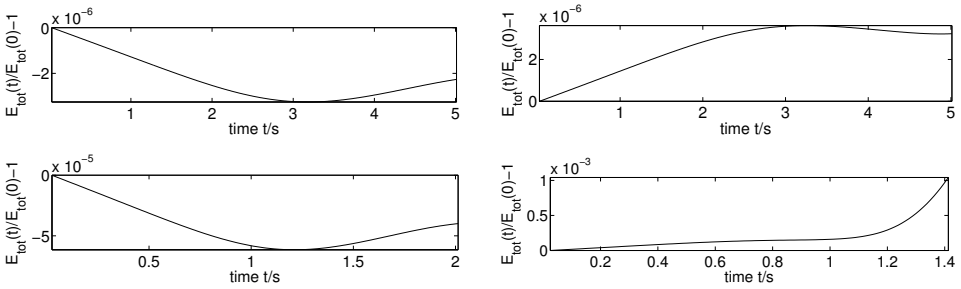

Figure 6.17: Relative error in total energy of the anelasic (left column) and pseudo-incompressible schemes (right column) for the falling cold air bubble; upper row: $\theta_{min}/\theta_{max} = 270\,\mathrm{K}/300\,\mathrm{K}$, lower row: $\theta_{min}/\theta_{max} = 90\,\mathrm{K}/300\,\mathrm{K}$.

called, first baroclinic effect, which merely changes even in case of high potential temperature variations, causes the stretching of the bubble when it falls down and is the reason for the stretching of the bubble in the anelastic case.

The first baroclinic effect is prominent in both the anelastic and the pseudo-incompressible models. In the latter model, however, a second baroclinic effect counteracts the first one, in particular for large potential temperature variations (see lower right panel of Figure 6.16). Here, the nonlinear pressure gradient term causes a vorticity production proportional to $\nabla\theta \times \nabla\pi$. This effect is not captured by the anelastic (or Boussinesq) model as $\nabla \times \nabla(\bar{\theta}\pi) = 0$. With a maximum pressure value at the bottom of the droplet which decreases with height, and with an outward pointing potential temperature gradient, there develop hence in the pseudo-incompressible case positive vorticity on the right and negative vorticity on the left of the symmetry axis, counteracting the stretching. Therefore, in the upper right panel with a relative small potential temperature variation, the stretching is dominate, but in case of a larger variation (lower right panel) the second baroclinic effect counteracts the stretching.

In general, our variational schemes represent well the first, and in case of the pseudo-

incompressible scheme also the second baroclinic effect for both mesh types. Our results agree well with those of [9] for low and for large potential temperature variations up to $\theta_{min}/\theta_{max} = 90\,\mathrm{K}/300\,\mathrm{K}$. As we do not apply flux limiters or any smoothing in our schemes (see also discussion in Section 6.2.1), we did not result in smooth solutions for the cold bubble test case with even higher potential temperature variations (as studied for instance by Klein [9]) when integrating the pseudo-incompressible scheme for more than 1.5 s. Here, too steep gradients in θ, which are strongly under-resolved on the front of the bubble, destroy the bubble's round shape. Moreover, this effect causes in both schemes, similarly to the warm bubble case, a decrease of the minimum θ value at the bubble's front of about 5 K for a variation of $\theta_{min}/\theta_{max} = 270\,\mathrm{K}/300\,\mathrm{K}$ and of about 20 K for $\theta_{min}/\theta_{max} = 90\,\mathrm{K}/300\,\mathrm{K}$.

Figure 6.17 shows, for regular meshes, the relative errors of total energy for the anelastic (left column) and pseudo-incompressible schemes for potential temperature profiles with $\delta\theta = 30\,\mathrm{K}$ (upper row) and $\delta\theta = 210\,\mathrm{K}$ (lower row). The values for total energy are well conserved while also here we realize for the pseudo-incompressible scheme a decrease in accuracy when the potential temperature gradients are too steep. For all cases, the values for mass, defined in equations (6.7) and (6.12), are very well conserved in the order of 10^{-14} (not shown). The relative errors obtain on irregular meshes are in the same order (also not shown).

7 Conclusion

In this paper, we derived variational integrators for the anelastic and pseudo-incompressible models by applying the variational discretization framework introduced in [14]. In order to enable the use of this framework, we first described the anelastic and pseudo-incompressible approximations of the Euler equations of a perfect gas in terms of the Euler-Poincaré variational method. Applying the idea of weighted volume forms, i.e. weighted in terms of the background stratifications of density (anelastic) or of density times potential temperature (pseudo-incompressible), we could identify the appropriate Lie group configuration space for the two models. The corresponding equations of motion follow by Hamilton's variational principle of stationary action.

The inclusion of the anelastic and pseudo-incompressible models into the theory of Euler-Poincaré variational method allows us to apply the variational discretization approach of Pavlov et al. [14]. In fact, we extended the latter by suitable discrete diffeomorphism groups, that incorporate the idea of weighted meshes as discrete counterparts of the weighted volume forms, in order to match the divergence-free conditions of the corresponding weighted velocity fields. Alongside, we defined appropriate weighted pairing required to derive the functional derivatives of the discrete Lagrangian that leads to the corresponding discrete equations of motion. Following this pathway, we could directly apply the flat operator of [14], which is a delicate issue otherwise. In this vein, we derived structure-preserving discretizations on irregular 2D simplicial meshes for the Boussinesq, anelastic, and pseudo-incompressible models.

We verified the structure-preserving properties of these variational integrators for both regular and irregular triangular meshes with respect to two test cases. In the hydrostatic adjustment process, we considered an atmosphere in which the vertically varying reference states are in hydrostatic balance. When out of this equilibrium, the system tends to a balanced state by emitting internal gravity waves subject to a model-dependent dispersion relation. Numerical simulations showed that each of our variational integrators capture very well the characteristics of the corresponding dispersion relation, in particular the upper and lower bounds of permitted

wave numbers. To test also the nonlinear behavior, we performed advection dominated tests using a warm rising, resp., cold falling bubble in a cold, resp., warm environment. Our variational integrators perform very well when compared with reference literature, in particular they capture nicely the shape and advection speed of the bubbles. In all these cases studied, both mass and energy are conserved to a high degree confirming the structure-preserving nature of our variational integrators.

Subject of our current work is the study of variational integrators for nonlinear rotating shallow-water equations. In this vein, it is our goal to extend the variational discretization framework in order to derive structure-preserving discretization for fully two and three dimensional compressible flows.

Acknowledgments. The authors thank D. Cugnet, M. Desbrun, F. Lott, and V. Zeitlin for helpful discussions and valuable feedback. Both authors were partially supported by the ANR project GEOMFLUID, ANR-14-CE23-0002-01. W. Bauer receives funding from the European Union's Horizon 2020 research and innovation programme under the Marie Skłodowska-Curie grant agreement No 657016.

References

[1] Abraham R. and Marsden J. E., *Foundations of mechanics*, Benjamin-Cummings Publ. Co., second edition, 1978.

[2] Bauer, W., Baumann, M., Scheck, L., Gassmann, A., Heuveline, V., and Jones, S. C. [2014], Simulation of tropical-cyclone-like vortices in shallow-water icon-hex using goal-oriented r-adaptivity, *Theoretical and Computational Fluid Dynamics*, **28(1)**, 107–128.

[3] Cotter, C., and Holm, D. [2014], Variational formulations of sound-proof models, *Quarterly Journal of the Royal Meteorological Society*, **140**(683), 1966 – 1973.

[4] Desbrun M., Gawlik E., Gay-Balmaz F., and Zeitlin V. [2014], Variational discretization for rotating stratified fluids, *Disc. Cont. Dyn. Syst. Series A*, **34**(2), 479–511.

[5] Durran, D. R. [1989], Improving the anelastic approximation, *J. Atmos. Sci*, **46**, 1453–1461.

[6] Durran, D. [1999], *Numerical Methods for Wave Equations in Geophysical Fluid Dynamics*, second edition, Springer-Verlag, New York.

[7] Gawlik, E. S., Mullen, P., Pavlov, D., Marsden, J. E., and Desbrun M. [2011], Geometric, variational discretization of continuum theories, *Physica D*, **240**(21), 1724–1760.

[8] Holm, D. D., J. E. Marsden, and T. S. Ratiu, [1998], The Euler-Poincaré equations and semidirect products with applications to continuum theories, *Adv. in Math.* **137**, 1–81.

[9] Klein, R., [2009], Asymptotics, structure, and integration of sound-proof atmospheric flow equations, *Theor. Comput. Fluid Dyn.*, **23**, 161–195.

[10] Lamb, H. [1932], Hydrodynamics, Ch. 309, 310, *Dover*.

[11] Lipps, F. and Hemler, R. [1982], A scale analysis of deep moist convection and some related numerical calculations, *J. Atmos. Sci.*, **29**, 2192–2210.

[12] J.E. Marsden and T.S. Ratiu, *Introduction to mechanics and symmetry*, Texts in Applied Math., **17**, Springer-Verlag.

[13] Ogura, Y. and Phillips, N. [1962], Scale analysis for deep and shallow convection in the atmosphere, *J. Atmos. Sci.*,**19**, 173–179.

[14] Pavlov, D., Mullen, P., Tong, Y., Kanso, E., Marsden, J. E., and Desbrun, M. [2010], Structure-preserving discretization of incompressible fluids, *Physica D*, **240**(6) (2010), 443–458.

[15] Wilhelmson, R. and Ogura, Y. [1972], The pressure perturbation and the numerical modeling of a cloud, *J. Atmos. Sci.*, **29**, 1295–1307.